Title

Regulated Proteolysis of MutSγ Controls Meiotic Crossing Over

Journal

Molecular Cell, 78(1)

ISSN

1097-2765

Authors

He, Wei
Rao, HBD Prasada
Tang, Shangming
et al.

Publication Date

2020-04-01

DOI

10.1016/j.molcel.2020.02.001

Peer reviewed

Published in final edited form as:

Mol Cell. 2020 April 02; 78(1): 168–183.e5. doi:10.1016/j.molcel.2020.02.001.

Regulated proteolysis of MutSγ controls meiotic crossing over

Wei He[1,2], **H.B.D. Prasada Rao**[1,2,†], **Shangming Tang**[1,2], **Nikhil Bhagwat**[1,2], **Dhananjaya S. Kulkarni**[1,2], **Yunmei Ma**[1,2], **Maria A.W. Chang**[2], **Christie Hall**[2], **Junxi Wang-Bragg**[2], **Harrison S. Manasca**[2], **Christa Baker**[2], **Gerrik F. Verhees**[2], **Lepakshi Ranjha**[4], **Xiangyu Chen**[3], **Nancy M. Hollingsworth**[3], **Petr Cejka**[4], **Neil Hunter**[1,2,5,6]

[1]Howard Hughes Medical Institute, University of California, Davis, Davis, California, USA [2]Department of Microbiology & Molecular Genetics, University of California, Davis, Davis, California, USA [3]Department of Biochemistry and Cell Biology, Stony Brook University, Stony Brook, New York, U.S.A. [4]Institute for Research in Biomedicine, Universita della Svizzera italiana, Bellinzona, Switzerland [5]Department of Molecular & Cellular Biology, University of California, Davis, Davis, California, USA [6]Department of Cell Biology & Human Anatomy, University of California, Davis, Davis, California, USA

SUMMARY

Crossover recombination is essential for accurate chromosome segregation during meiosis. The MutSγ-complex, Msh4-Msh5, facilitates crossing over by binding and stabilizing nascent recombination intermediates. We show that these activities are governed by regulated proteolysis. MutSγ is initially inactive for crossing over due to an N-terminal degron on Msh4 that renders it unstable by directly targeting proteasomal degradation. Activation of MutSγ requires the Dbf4-dependent kinase, Cdc7 (DDK), which directly phosphorylates and thereby neutralizes the Msh4 degron. Genetic requirements for Msh4 phosphorylation indicate that DDK targets MutSγ only after it has bound to nascent JMs in the context of synapsing chromosomes. Overexpression studies confirm that the steady-state level of Msh4, not phosphorylation perse, is the critical determinant for crossing over. At the DNA level, Msh4 phosphorylation enables the formation and crossover-biased resolution of double-Holliday Junction intermediates. Our study establishes regulated protein degradation as a fundamental mechanism underlying meiotic crossing over.

Graphical Abstract

*Correspondence to lead contact: Neil Hunter, nhunter@ucdavis.edu.
†Current address: National Institute of Animal Biotechnology, Hyderabad, Telangana, India.

AUTHOR CONTRIBUTIONS

W.H. and N.H. conceived the study and designed most experiments. L.R. and P.C. purified MutSγ derivatives. N.M.H., X.C. and W.H. designed *in vitro* kinase experiments. All authors performed experiments and analyzed the data. W.H. and N.H. wrote the manuscript with inputs and edits from all authors.

SUPPLEMENTAL INFORMATION

Supplemental Information includes 10 figures, 8 tables.

DECLARATION OF INTERESTS

The authors declare no competing interests.

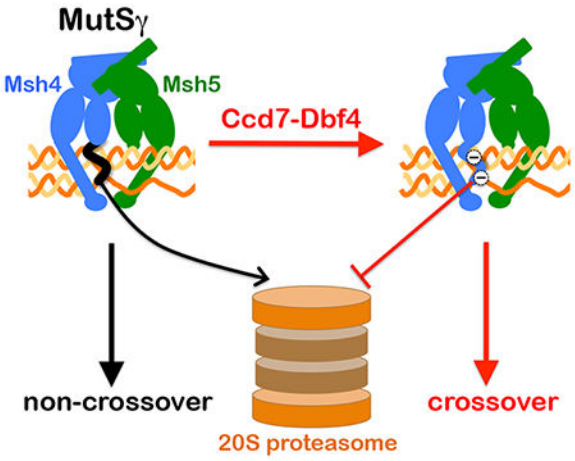

Keywords

Meiosis; chromosome; homologous recombination; crossing over; aneuploidy; MutS; proteasome; Cdc7; Holliday Junction; degron

INTRODUCTION

Crossover recombination connects homologous chromosomes to promote their accurate segregation during the first division of meiosis. Defects in crossing over cause infertility, miscarriage and congenital disease (Hunter, 2015). A fundamental question in meiosis is how crossovers are differentiated from a larger pool of precursor recombination sites in such a way that each pair of chromosomes becomes connected by at least one crossover, despite a low total number of crossovers per nucleus (Jones, 1984).

Meiotic recombination is initiated by Spoil-catalyzed DNA double-strand breaks (DSBs) (Lam and Keeney, 2014), which outnumber crossovers by ~2-fold in budding yeast, ~10-fold in mammals and up to 30-fold in some plants. Analysis of joint-molecule (JM) recombination intermediates in budding yeast together with fine-scale analysis of recombination products in a variety of species, indicates that crossover and non-crossover pathways diverge following DSB resection and initial DNA strand exchange to form nascent displacement loops (D-loops)(Hunter, 2015). A majority of noncrossovers arise from D-loops via synthesis-dependent strand annealing in which the invading 3’ end is extended by DNA polymerase, unwound and then annealed to the other DSB end. Crossovers form via a distinct pathway involving metastable one-ended strand-exchange intermediates called single-end invasions (SEIs)(Hunter and Kleckner, 2001); through DNA synthesis and capture of the second DSB end, SEIs give rise to double Holliday Junctions (dHJs), which must then undergo biased resolution into crossovers (Zakharyevich et al., 2012).

At the cytological level, prospective crossover sites selectively retain specific recombination factors such as the MutSγ complex, Msh4-Msh5. This patterning process is dependent on the SUMO-modification and ubiquitin-proteasome systems suggesting a model in which factors such as MutSγ are selectively stabilized at crossover sites by protecting them from

proteolysis (Agarwal and Roeder, 2000; Ahuja et al., 2017; De Muyt et al., 2014; Nguyen et al., 2018; Qiao et al., 2014; Rao et al., 2017; Reynolds et al., 2013; Yokoo et al., 2012; Zhang et al., 2018). MutSγ specifically binds a variety of JM structures *in vitro*, and stabilizes Holliday Junctions in the stacked-X conformation, which is refractory to branch migration (Lahiri et al., 2018; Snowden et al., 2004). *In vivo*, MutSγ is thought to promote the formation and/or crossover-biased resolution of dHJs (De Muyt et al., 2014; Franklin et al., 2006; Reynolds et al., 2013; Yokoo et al., 2012; Zhang et al., 2014; Manhart and Alani, 2016; Pochart et al., 1997; Snowden et al., 2004).

Here, we confirm that regulated proteolysis plays a direct and essential role in meiotic crossing over, identify a specific target, and delineate an unusual mechanism. Msh4 is identified as an intrinsically unstable protein that is directly targeted for proteasomal degradation by an N-terminal degron, thereby rendering MutSγ inactive for its crossover functions. Activation occurs by neutralizing the Msh4 degron via phosphorylation, catalyzed by the conserved cell-cycle kinase, Cdc7-Dbf4 (DDK). Thus, a key meiotic pro-crossover factor is activated by attenuating its proteolysis.

RESULTS

Phosphorylation is Essential for the Crossover Function of Msh4

The ZMM proteins were surveyed for modifications detectable as electrophoretic-mobility shifts on Western blots. A prominent modified band was detected for Msh4 but not for its partner Msh5 (Figure 1A and Supplemental Information Figure S1). Treatment of immunoprecipitated Msh4 with λ phosphatase indicated that the modified form is due to phosphorylation (Figure 1B). Relative to the unphosphorylated protein, phosphorylated Msh4 appeared with a ≥1 hr delay, its levels peaked at ~22% of total protein, and then both species disappeared with the same timing (Supplemental Information Figure S1). To map sites of phosphorylation, Msh4 was immunoprecipitated, fast and slow migrating forms were resolved by electrophoresis, and then analyzed separately by tandem mass spectrometry (MS/MS; Figure 1C and Supplemental Information Figure S1). Six phosphorylation sites were identified in the slower migrating form of Msh4, all mapping within the first 50 amino acids (S2, S4, S7, S41, T43 and S46; Figure 1C; Supplemental Information Figure S1). In the faster migrating form of Msh4, only phosphorylation at S41 was detected.

Msh4 and Msh5 lack the N-terminal domain I, which is conserved in other MutS proteins (Figure 1C and 1D). Domain I encircles DNA together with MutS domain IV and is intimately involved in DNA binding and mismatch recognition (Yang et al., 2000). Absence of domain I from Msh4 and Msh5 is predicted to enlarge the DNA channel such that it can accommodate JM structures and slide on two duplexes (Rakshambikai et al., 2013; Snowden et al., 2004). The functions of the N-terminal regions of Msh4 and Msh5 are otherwise unknown.

To assess whether phosphorylation is required for the crossover function of Msh4, we mutated the six identified phosphorylation sites to alanine to prevent phosphorylation, or to aspartic acid to mimic phosphorylation, creating respectively *msh4-6A* and *msh4-6D* alleles. Genetic map distances were then measured in a background carrying markers on three

different chromosomes (III, VII and VIII; Figure 1E). Cumulative map distances showed that *msh4*Δ reduced crossing by 2.1 to 2.7-fold (Figure 1F; Supplemental Information Figure S2 and Table S2). Similar reductions (2.1 to 2.8-fold) were seen for the *msh4-6A* phosphorylation-defective strain. Thus, phosphorylation is essential for the crossover function of Msh4. For chromosomes VII and VIII, the *msh4-6A* mutation caused slightly larger reductions in crossing over than the *msh4*Δ null. Possibly, phosphorylation-defective msh4-6A protein is still capable of binding recombination intermediates thereby impeding processing via alternative crossover pathways mediated by the structure-selective nucleases (De Muyt et al., 2012; Zakharyevich et al., 2012). By contrast, in the phospho-mimetic *msh4-6D* strain, cumulative map distances were indistinguishable from those of wild type. The contributions of individual phosphorylation sites to the crossover function of Msh4 were also assessed. This analysis revealed a major role for sites S2, S4 and S7, while S41, T43 and S46 made little or no contribution (Supplemental Information Figure S3). Western analysis indicated that msh4-6A protein could still be phosphorylated, albeit with a delay and at lower levels than wild-type Msh4 (low-level phosphorylation was also detected for msh4-6D; Figure 4A; also see Supplemental Information Figure S6). This residual phosphorylation was abolished following mutation of all 18 serine and threonine residues present in the first 50 amino acids of Msh4 indicating that phosphorylation leading to the slow migrating form is confined to this to this region. Importantly, the *msh4-18A* strain was no more defective for crossing over than the *msh4-6A* strain, indicating that phosphorylation at other sites in the N-terminus is not functionally redundant with the phosphorylation sites mapped by MS/MS (Supplemental Information Figure S3).

Next, we determined whether crossover assurance is influenced by Msh4 phosphorylation using a strain carrying eight linked intervals that span the length of chromosome III (Figure 1F and Supplemental Information Table S5)(Zakharyevich et al., 2010). In wild type, at least one crossover was detected in 98.9% of tetrads indicating highly efficient crossover assurance. Oppositely, crossover assurance was severely defective in the absence of Msh4, with 25.2% of *msh4*Δ tetrads lacking a detectable crossover on chromosome III, consistent with previous analysis (Krishnaprasad et al., 2015). In addition, the fraction of tetrads with a single crossover was increased and multiple crossover classes were diminished in the *msh4*Δ strain relative to wild type ($P<0.001$, *G*-test). If crossover assurance remained operational in *msh4-6A* cells, the average residual crossover frequency along chromosome III (1.7 crossovers per meiosis) would be sufficient to ensure ≥1 crossover per meiosis. However, 17.4% of *msh4-6A* tetrads had zero crossovers indicating an essential role for Msh4 phosphorylation in crossover assurance (Figure 1F; $P<0.001$ compared to wild type, *G*-test; distributions of crossover classes were not discernably different for *msh4-6A* and msh4Δ, $P=0.38$). By contrast, crossover assurance remained efficient in *msh4-6D* cells ($P=0.79$ relative to wild type, *G*-test). In conclusion, phosphorylation of the N-terminus of Msh4 promotes the formation of crossovers that result in crossover assurance. Additional analysis shows that the crossovers facilitated by Msh4 phosphorylation are also patterned by interference (Supplemental Information Figure S2 and Tables S3 and S4).

In the absence of Msh4, defective crossing over causes chromosome missegregation resulting in spore death (Krishnaprasad et al., 2015; Nishant et al., 2010; Novak et al., 2001; Stahl et al., 2004). Consistent with previous studies, *msh4*Δ reduced spore viability to 34.7%

and the pattern of spore death was indicative of chromosome missegregation at the first meiotic division, with a preponderance of tetrads containing two or zero viable spores (Figure 1G; Supplemental Information Figure S2 and Table S1)(Krishnaprasad et al., 2015; Nishant et al., 2010; Novak et al., 2001; Stahl et al., 2004). The pattern of spore death in cells carrying the phosphorylation-defective *msh4-6A* allele was similar to that of the *msh4*Δ null, with an overall viability of 46.7% ($P<0.01$ compared to wild type, χ^2 test). By contrast, the phospho-mimetic *msh4-6D* allele supported wild-type levels of spore viability (96.3% and 95.7%, respectively, $P=0.42$).

Previous analysis showed that non-crossover gene conversions are increased in the absence of ZMMs, including Msh5 (and by extension Msh4), due to the continued formation of DSBs when homolog engagement is defective (Hollingsworth et al., 1995; Novak et al., 2001; Thacker et al., 2014). This phenotype was reflected in tetrad data from the *msh4*Δ null strain, which showed a 3.4-fold increase in cumulative gene conversion frequency (Supplemental Information Figure S4). Elevated gene conversion was also seen for *msh4-6A*, which showed a 2.5-fold increase in gene conversions relative to wild type. Unexpectedly, a 1.7-fold increase in gene conversion was observed for the *msh4-6D* strain, the first indication that this phospho-mimetic allele is not fully wild type.

Msh4 Phosphorylation Facilitates the Formation and Resolution of DNA Joint Molecules

To understand how the molecular steps of meiotic recombination are influenced by Msh4 phosphorylation, DNA intermediates were monitored in cultures undergoing synchronous meiosis using a series of Southern blot assays at the *HIS4::LEU2* recombination hotspot (Figure 2)(Hunter and Kleckner, 2001; Oh et al., 2007).

In *msh4-6A* cells, DSB repair, progression of recombination and meiotic divisions were all delayed relative to wild type (Figure 2A, B and C). Similar but more severe defects were seen for *msh4Δ*. Consistent with our genetic analysis (Figure 1F), crossovers at *HIS4::LEU2* were reduced ~2-fold in both *msh4-6A* and *msh4*Δ cells (Figure 2C). In *msh4-6D* cells, slight delays (<20 minutes) in DSB turnover and crossover formation were apparent, but crossovers reached wild-type levels.

The increased frequencies of gene conversion seen in *msh4*Δ and *msh4-6A* tetrads were mirrored by elevated levels of non-crossover gene conversions at *HIS4::LEU2* (Supplemental Information Figure S4). Again, the effect of *msh4-6A* was weaker than that of the *msh4*Δ null (increases of 1.8-fold versus 3.0-fold, respectively). Although gene conversion was also significantly elevated in *msh4-6D* tetrads, non-crossovers at *HIS4::LEU2* were not significantly increased.

Two-dimensional gel analysis revealed the importance of Msh4 phosphorylation for JM metabolism (Figure 2D–G). In *msh4-6A* cells, appearance of all JM species was delayed by ~30-60 min compared to wild type. A further delay of ~1.5 hrs was seen for the disappearance of JMs. Peak JM levels were also lower in *msh4-6A* cells, averaging 61% of wild-type levels (Figure 2G). JM kinetics in *msh4*Δ null mutants were similar to those of *msh4-6A* (Figure 2F), but peak JM levels were significantly lower averaging just 40% of wild-type levels (Figure 2G). Thus, with respect to DSB persistence, JM levels and prophase

delay, the phenotypes of the *msh4-6A* mutant are milder than those of the *msh4*Δ null, consistent with partial function of the phosphorylation defective msh4-6A protein for JM formation.

Notably, SEIs reached similar levels in *msh4-6A* and *msh4*Δ cells (% of hybridizing DNA = 1.19% ± 0.05 S.E. and 0.91% ± 0.13 S.E., respectively), but dHJ levels were ~2-fold lower in *msh4*Δ cells (0.83% ± 0.05 S.E. and 0.40% ± 0.02 S.E., respectively; $p<0.01$; Students *t*-test; Figure 2G). Two non-exclusive possibilities could explain this difference: (i) the SEI-to-dHJ transition is more efficient and/or (ii) the stability of IH-dHJs is higher in the presence of msh4-6A than when Msh4 is absent. However, despite higher IH-dHJ levels in *msh4-6A* versus *msh4*Δ, crossovers were reduced by the same extent in both strains (Figures 1E and 2C). In *msh4-6D* cells, a minor delay in SEI formation was observed and IH-dHJs peaked at ~24% higher levels than wild type (1.58% ± 0.11 versus 1.27% ± 0.11), but otherwise, kinetics and levels of JMs in *msh4-6D* cells were similar to those of wild type (Fig 2F and G). Together, our JM analysis suggests that phosphorylation of Msh4 is important both for JM formation and the biased resolution of IH-dHJs into crossovers.

Phosphorylation Promotes Chromosomal Localization of Msh4

To begin to understand how phosphorylation facilitates Msh4 function, the chromosomal localization patterns of Msh4, msh4-6A and msh4-6D proteins were compared. Surface spread nuclei were immunostained for both Msh4 and Zip1 (Figure 3A and 3B). Msh4 foci were quantified in nuclei with zygotene (class II) and pachytene (class III) morphologies, i.e. partial and complete lines of Zip1 staining. In wild-type, Msh4 foci averaged 43.9 ± 13.3 S.D. per nucleus while focus numbers in *msh4-6A* nuclei were lower, averaging 33.8 ± 10.4 S.D. ($P<0.0001$, two-tailed Mann Whitney test; Figure 3B). By contrast, the msh4-6D protein formed slightly elevated numbers of foci relative to wild-type Msh4, averaging 47.7 ± 11.3 S.D. per nucleus ($P=0.028$). Phenotypes associated with phosphorylation-defective (*msh4-3A*) and phosphorylation-mimetic (*msh4-3D*) alleles for sites S2, S4 and S7 were analogous to those of *msh4-6A* and *msh4-6D* with respect to formation of Msh4 foci (Supplemental Information Figure S5), further highlighting the importance of these three proximal serine residues. Thus, phosphorylation facilitates the chromosomal localization of Msh4 into immunostaining foci.

Msh4 Phosphorylation Facilitates Homolog Synapsis

In many species, the homology search and strand-exchange steps of recombination promote homolog pairing and SC formation (Zickler and Kleckner, 2015). Crossovers then mature in the context of SCs. The possibility that the inefficient JM formation and decreased Msh4 foci seen in *msh4-6A* cells leads to defective homolog synapsis was addressed by immuno-staining surface-spread nuclei for the SC component Zip1. Synapsis was quantified over time by assigning nuclei to one of three Zip1 staining classes (Borner et al., 2004): class I nuclei had a dotty pattern; class II had partial synapsis with both linear and dotty staining; and class III had full synapsis indicated by extensive linear staining (Figure 3C and Supplemental Information Figure S5). Nuclei containing aggregates of Zip1 called polycomplexes (PCs), a sensitive indicator of synapsis defects (Sym and Roeder, 1995), were also quantified.

Consistent with previous studies (Borner et al., 2004; Novak et al., 2001), synapsis was severely defective in *msh4*Δ cells; class III nuclei with full synapsis peaked at only 9% (compared to 35% of wild-type nuclei) and PCs were present in the majority of cells (Figure 3D). PCs were similarly prominent in *msh4-6A* cells, but synapsis was slightly more efficient than *msh4*Δ, with higher levels of class II and class III nuclei ($P<0.005$, *G*-test). By contrast, synapsis in *msh4-6D* cells was indistinguishable from wild type ($P = 0.63$). Thus, Msh4 phosphorylation promotes the formation and/or stabilization of SCs.

Msh4 is Stabilized by Phosphorylation

We explored the possibility that aberrant localization of phosphorylation-defective msh4-6A protein is caused by decreased protein stability. Consistent with this idea, Western analysis showed that msh4-6A protein levels were lower at all time points during meiosis, averaging a 2.2-fold reduction relative to wild-type Msh4 (Figure 4A and 4B; and Supplemental Information Figure S6). In contrast, the msh4-6D protein was hyper-stable, with an average increase of 2.1-fold.

The inference that Msh4 is subject to phospho-regulated proteolysis was supported by the observation that proteasome inhibition with MG 132 restored msh4-6A to wild-type levels (Figure 4C and 4D). Wild-type and *msh4-6A* cells were treated with the proteasome inhibitor MG132 two hours after transfer to sporulation medium and Msh4 protein levels were measured at 4, 5 and 6 hrs by Western blot (Figure 4C). In the absence of MG 132, msh4-6A protein levels were reduced to 21-44% of wild-type levels. Treatment with MG132 restored msh4-6A levels to between 94% and 125% of Msh4 levels seen in control wild-type cells (Figure 4D). MG132 treatment did not have a significant effect on wild-type Msh4 levels at 4 and 5 hrs, but at 6 hrs levels were 1.8-fold higher than in untreated cells. Unexpectedly, the phosphorylated form of wild-type Msh4 was diminished following MG132 treatment (Figure 4C). We suspect that this is due to the synapsis defects caused by proteasome inhibition (Ahuja et al., 2017; Rao et al., 2017), which is consistent with our analysis below showing that SC component Zip1 is required for Msh4 phosphorylation (Figure 7B). Regardless, MG 132 has a differential effect on the turnover of the phosphorylation-defective msh4-6A protein relative to wild-type Msh4. These data suggest that phosphorylation stabilizes Msh4 during meiotic prophase I by protecting it from proteasomal degradation.

If the primary function of phosphorylation is to stabilize Msh4, then high levels of phosphorylation-defective msh4-6A protein might bypass the requirement for phosphorylation. Strikingly, overexpression of *msh4-6A* using the strong, copper-inducible *CUP1* promoter (Figure 4E) supported high levels of crossing-over and restored spore viability to near wild-type levels (Figure 4F and 4G). In fact, crossover levels in cells overexpressing msh4-6A were 29% higher than those of control wild-type cells, consistent with the interpretation that the steady-state level of Msh4, and not Msh4 phosphorylation *per se*, is a major determinant of crossing over.

To understand how Msh4 levels influence the formation of MutSγ complexes, levels of Msh4 and Msh5 were measured in whole cell extracts from wild-type, *msh4-6A, msh6D* and P_{cup1}-*msh46A* strains; and relative efficiencies of MutSγ complex formation were inferred

by measuring the amount of Msh4 that co-immunoprecipitated with Msh5 (Figure 4H and 4I; and Supplemental Information Figure S6). Despite a 9.4-fold range of Msh4 levels in these four strains, Msh5 levels remained constant. In cells expressing the unstable msh4-6A protein, the relative efficiency of MutSγ complex formation was 2.6-fold lower than that of wild-type cells (Figure 4H and 4I). In P_{cup1}-*msh4-6A* strains, MutSγ complexes were restored to wild-type levels revealing how overexpression of unstable msh4-6A supports high levels of crossing over.

Wild-type MutSγ levels were also observed in cells expressing hyper-stable phosphomimetic msh4-6D protein (Figure 4H and 4I). However, in contrast to the hyper-crossover phenotype of P_{cup1}-*msh46A* strains (Figure 4F), crossover levels in *msh4-6D* strains were not higher than wild type (Figure 1 and Supplemental Figure S2). To understand this discrepancy, we examined the abilities of purified MutSγ complexes containing phosphomimetic msh4-3D and msh4-6D proteins to bind to model Holliday Junction (HJ) substrates *in vitro* (Figure 4J and 4K). By EMSA, both Msh4(3D)-Msh5 and Msh4(6D)-Msh5 complexes bound HJs less efficiently than wild-type MutSγ, by 2.8- and 5.2-fold respectively. These data suggest that the hyperstability of phosphomimetic msh4-3D and msh4-6D *in vivo* may be offset by a reduced ability to bind JM intermediates such that crossing over is not elevated. Consistent with this interpretation, P_{cup1}-*MSH4* strains, overexpressing wild-type Msh4 protein, formed 26% more crossovers than *MSH4* control cells (Figure 4L).

The Msh4 N-Terminus Encodes a Portable Degron That Directly Targets Proteasomal Proteolysis

Our analysis points to a model in which Msh4 is an intrinsically unstable protein that is stabilized by phosphorylation of N-terminal residues to form MutSγ complexes that are sufficiently long-lived to effect crossing over. To determine whether the N-terminal region confers intrinsic instability to Msh4, full-length protein and an N-terminally truncated derivative (Msh4-ΔN50) were co-expressed in vegetative (non-meiotic) cells (Figure 5A–C). Levels of full-length Msh4 were 3-fold lower than those of Msh4-ΔN50 and MG 132 treatment showed that this difference was due to proteasomal degradation. By contrast, the N-terminus of Msh5 had no effect on its stability (Supplemental Information Figure S7). Comparison of protein levels in strains co-expressing msh4-6D and Msh4-ΔN50, or wild-type Msh4 and Msh4-ΔN50 revealed that phospho-mimetic S/T-D mutations attenuated N-terminal degron activity (Figure 5D–F). Protein half-lives, estimated from cycloheximide chase experiments, were ~14, 31 and 61 minutes respectively for Msh4, msh4-6D and Msh4-ΔN50 (Supplemental Information Figure S8). Autonomous, portable degron activity of the Msh4 N-terminus was demonstrated by fusing residues 1–50 to GFP and co-expressing this Degron-GFP construct together with wild-type GFP (Figure 5G–I and Supplemental Information Figure S8). The Msh4 degron destabilized GFP, reducing its half-life from ~59 to 19 mins. By contrast, stability of a phospho-mimetic Degron(6D)-GFP fusion was similar to that of wild-type GFP (half life of ~49 mins). Together, these data indicate that the N-terminal domain of Msh4 comprises an autonomous degron that is neutralized by phosphorylation.

Failure to detect ubiquitylated forms of the Degron-GFP fusion (not shown) raised the possibility that Msh4 is directly targeted for proteasomal degradation (Jariel-Encontre et al., 2008). Consistently, a degron lacking the four potential ubiquitin acceptor lysines (KODegron) was indistinguishable from the wild-type degron with respect to destabilization of GFP; and further mutation of the 19 lysines in GFP (KODegron-KOGFP) ruled out the possibility that GFP was being ubiquitylated (Figure 5J–L). Incubation of purified MutSγ with 20S proteasomes *in vitro* confirmed that Msh4, but not Msh5, is a direct target of proteasomal degradation with a half-life of ~14 mins, identical to that observed *in vivo* (Figure 5M and 5N). Thus, while Msh4 is subject to regulated proteasomal proteolysis, this can occur without ubiquitin and/or SUMO modification.

Msh4 Phosphorylation is Catalyzed by Dbf4-Dependent Kinase, Cdc7

To identify the kinase(s) responsible for Msh4 phosphorylation, we systematically analyzed candidate kinases (Figure 6 and Supplemental Information Figure S9). $Mec1^{ATR}$ and $Tel1^{ATM}$ are primary sensor kinases for the DNA-damage response and regulate various aspects of meiotic recombination (Subramanian and Hochwagen, 2014). Although $Mec1^{ATR}$/$Tel1^{ATM}$ were required for Msh4 phosphorylation (Supplemental Information Figure S9), identified modification sites are not S/T-Q consensus sequences making Msh4 unlikely to be a direct target. Similarly, the downstream effector kinase, Mek1 (Subramanian and Hochwagen, 2014), was required for Msh4 phosphorylation, but neither Msh4 nor Msh5 were direct targets of Mek1 *in vitro* (Supplemental Information Figure S9). Moreover, mapped phosphorylation sites do not match the Mek1 consensus (RXXT).

Dbf4-dependent kinase (DDK, comprising Cdc7 and Dbf4) regulates multiple aspects of meiotic prophase including DSB formation and synapsis (Chen et al., 2015; Matsumoto and Masai, 2013). DDK preferentially targets serines and threonines immediately upstream of a negative charge, which can be conferred either by negatively-charged amino acids or by phosphorylation. By these criteria, Msh4 S2, S7 and S46 are candidate DDK sites (Figure 1C). Inhibition of an analog-sensitive *cdc7-as* allele (after Cdc7 has activated DSB and SC formation) diminished phosphorylation of Msh4 and reduced its levels (Figure 6A and 6B). DDK and MutSγ interacted in solution (Figure 6C), and *in vitro* phosphorylation showed that DDK directly phosphorylates the N-terminus of Msh4, specifically at the sites identified by mass spectrometry (Figure 6D and Supplemental Information Figure S10). Moreover, DDK attenuated the proteasomal degradation of Msh4 *in vitro*, increasing its half-life from ~15 mins to >60 mins (Figure 6E and 6F).

Evidence That Msh4 Phosphorylation Occurs *In Situ* At Sites of Recombination

To understand how Msh4 phosphorylation is coupled to the key events of meiotic prophase, the genetic requirements for Msh4 phosphorylation were delineated using mutant strains defective for successive steps of recombination, chromosome pairing and synapsis (Figure 7A). Spo11 initiates recombination by catalyzing DSB formation (Lam and Keeney, 2014). Mnd1 is an essential co-factor for DNA strand-exchange (Brown and Bishop, 2015). Zip1 is the major component of SCs, assembling into linear oligomeric structures that connect homologous chromosomes and facilitate crossing over (Sym et al., 1993). In *zip1Δ* cells, initial DNA strand exchange and homolog pairing ensue, but synapsis is abolished and JM

maturation and crossing over are defective (Borner et al., 2004). Ecm11-Gmc2 comprises the central element of SCs (Humphryes et al., 2013; Voelkel-Meiman et al., 2013). Abnormal, patchy Zip1 structures are formed in *ecm11Δ/gmc2Δ* mutants, but crossovers form at high levels (Voelkel-Meiman et al., 2016). SUMO E3 ligase, Zip3, accumulates at prospective crossover sites and facilitates synapsis and the loading of pro-crossover factors, including MutSγ (Agarwal and Roeder, 2000; Cheng et al., 2006; Shinohara et al., 2008). *zip3Δ* mutants are defective for synapsis, JM maturation and crossing over (Agarwal and Roeder, 2000; Borner et al., 2004). Msh4 phosphorylation was not detected in *spo11-Y135F* (catalytically dead), *mnd1Δ, zip1Δ* and *zip3Δ* mutants. By contrast, phosphorylation of Msh4 reached wild-type levels in *ecm11Δ* cells, indicating that full synapsis is not required (Figure 7B).

Analysis of two additional mutants showed that Msh4 phosphorylation is coincident with the formation of dHJs, but does not require their resolution into crossovers (Figure 7A). Cells lacking the transcription factor Ndt80 arrest with fully synapsed chromosomes and unresolved dHJs (Allers and Lichten, 2001). In *ndt80Δ* cells, phospho-Msh4 accumulated to very high levels (>60% of total Msh4) and persisted in arrested cells (Figure 7B). Mlh3 is a component of MutLγ, an endonuclease that promotes crossover-biased resolution of dHJs (Manhart and Alani, 2016). Phosphorylation of Msh4 appeared normal in *mlh3Δ* cells. The analysis above implies that Msh4 is phosphorylated *in situ* at sites of recombination after MutSγ has bound nascent JMs in the context of the nascent SC. Consistent with this inference, chromatin-associated Msh4 was highly enriched for the phosphorylated form relative to soluble Msh4 (Figure 7C).

DISCUSSION

Our findings identify an important mechanism underlying the enigmatic process of meiotic crossover/non-crossover differentiation, and point to a model in which the stability of MutSγ complexes bound to nascent JMs determines whether they will mature into crossovers.

Regulated Proteolysis Is A Key Aspect of Meiotic Crossing Over

The molecular mechanisms that underpin the differentiation of meiotic crossover and noncrossover pathways have remained elusive. Specifically, it is not known how events leading to dHJ formation are facilitated at some recombination sites but not at others, and how dHJs maintain their crossover fate and undergo crossover-biased resolution. Here, regulated proteolysis is revealed as a key determinant of crossing over, with MutSγ stability being determined by a phospho-regulated degron that targets Msh4 for ubiquitin-independent proteasomal proteolysis. This discovery substantiates previous studies implicating proteasomal degradation in crossover/non-crossover differentiation (Ahuja et al., 2017; Qiao et al., 2014; Rao et al., 2017; Reynolds et al., 2013). Notably, when proteasomes are inactivated in mouse spermatocytes, meiotic recombination stalls and ZMM factors (including MutSγ) persist at sites that would normally mature into non-crossovers, suggesting that ZMMs may be targeted for proteolysis at these sites (Rao et al., 2017). At least one ZMM factor, Msh4, can now be designated as a direct target of proteasomal

degradation. Moreover, the atypical mode of Msh4 regulation reveals unanticipated facets of crossover differentiation: intrinsic instability of an essential crossover factor dictates that non-crossover will be the default outcome; and kinase-dependent stabilization activates crossing over.

The Crossover Activity of MutSγ Is Activated by Stabilizing Msh4

Distinct activities of the ZMMs influence different aspects of crossover maturation and couple these events to homolog synapsis. The DNA helicase, Mer3, functions both to regulate the extension of nascent D-loops by DNA synthesis, and to stabilize JMs (Borner et al., 2004; Duroc et al., 2017; Mazina et al., 2004; Nakagawa and Kolodner, 2002); the XPF-ERCC1 related complex, Zip2-Spo16, specifically binds JMs (De Muyt et al., 2018; Guiraldelli et al., 2018; Macaisne et al., 2011); Zip1 acts both locally to promote ZMM function and globally as the major component of SCs (Chen et al., 2015; Sym et al., 1993; Voelkel-Meiman et al., 2015); Zip3 is a SUMO E3 ligase that helps localize other ZMMs to nascent crossover sites and facilitates synapsis (Agarwal and Roeder, 2000; Cheng et al., 2006; Macqueen and Roeder, 2009; Shinohara et al., 2008); and Zip4 is a large TPR repeat protein thought to bridge interactions between Zip2-Spo16, Zip3, MutSγ and the chromosome axis protein Red1 (De Muyt et al., 2018). Several activities are ascribed to MutSγ: (i) specific binding and stabilization of nascent JMs (Lahiri et al., 2018; Snowden et al., 2004); (ii) protection of dHJs from the anti-crossover “dissolution” activity of the STR decatenase complex, Sgs1–Top3–Rmi1 (equivalent to the human BTR complex, BLM–TOPIIIαΔRMI1/2)(Jessop et al., 2006; Kaur et al., 2015; Oh et al., 2007; Tang et al., 2015) (Tang and Hunter, unpublished); (iii) direct or indirect recruitment and activation of crossover-biased JM resolving factors such as the MutLγ endonuclease (Manhart et al., 2017; Nishant et al., 2008; Ranjha et al., 2014; Zakharyevich et al., 2012); and (iv) formation and/or stabilization of homolog synapsis (Borner et al., 2004; Novak et al., 2001) (Tang and Hunter, unpublished).

Phosphorylation-defective msh4-6A protein can still localize to chromosomes and retains significant function for both synapsis and JM formation. However, the essential crossover function(s) of MutSγ is inactive unless Msh4 is stabilized via phosphorylation. We suggest that these essential functions are to protect nascent JMs from the anti-crossover “dissolution” activity of the STR decatenase complex, Sgs1–Top3–Rmi1 (equivalent to the human BTR complex, BLM–TOPIIIα–RMI1/2)(Kaur et al., 2015; Tang et al., 2015), and facilitate crossover-biased resolution of dHJs. This proposal is also consonant with our inference that DDK targets MutSγ complexes that have bound JMs in the context of synapsing chromosomes. Notably, STR/BTR complexes also accumulate at crossover sites (Jagut et al., 2016; Rockmill et al., 2003; Woglar and Villeneuve, 2018); and the symmetric arrangement of dual foci of MutSγ and BTR observed in C. *elegans* suggests a specific model in which MutSγ sliding clamps accumulate between the two junctions of a dHJ to impede dissolution into a non-crossover (Woglar and Villeneuve, 2018). Mechanistically, MutSγ appears to stabilize HJs in their stacked X conformation, which renders them refractory to branch migration (Lahiri et al., 2018), but likely also functions as a sliding clamp downstream of initial JM binding to stabilize JMs and recruit resolution factors (Milano et al., 2019; Snowden et al., 2004).

We suggest that sliding clamps of MutSγ must accumulate above a minimum number to ensure crossing over, be it through dHJ stabilization, recruitment or activation of resolving enzymes, or by maintaining dHJs in a geometry that is conducive to crossover-biased resolution. Under this model, the requisite threshold of dHJ-bound MutSγ clamps requires the stabilization of Msh4 by phosphorylation. We note that the estimated half-life of stabilized Msh4 (30–60 mins) is similar to the estimated lifespan of dHJs (Allers and Lichten, 2001; Hunter and Kleckner, 2001) suggesting a causal relationship.

If MutSγ were the sole limiting crossover factor for crossing over, then strains overexpressing Msh4 (as analyzed in Figure 4F and 4L) might be expected to show more than the observed 26–29% increase in crossing over. Thus, some additional factor(s) must limit crossover numbers. One possibility is that crossover numbers are limited by interference, and stabilization of Msh4 occurs downstream of the initial crossover patterning process. However, the proteolysis mechanism revealed here for Msh4 could be a more general mechanism, possibly coupled to interference, to regulate the availability of other essential crossover factors.

We further suggest that the intrinsic instability of Msh4 may be locally enhanced by proximity to proteasomes, which are recruited in high numbers along chromosome axes as they synapse (Ahuja et al., 2017; Rao et al., 2017). This SC-associated population of proteasomes could accelerate the loss of MutSγ from sites where Msh4 is not stabilized by phosphorylation and thereby drive recombination at most sites towards a non-crossover outcome.

Whether MutSγ is similarly regulated in other organisms remains unclear. An N-terminal region appears to be common to all Msh4 proteins, but sequence conservation is low. However, these regions are typically S/T rich, contain candidate DDK sites and are predicted to undergo disorder-enhanced phosphorylation (Supplemental Information Table S8).

Msh4 Is An Ubiquitin-Independent Target of Proteasomes

Msh4 adds to a growing list of proteins that can be directly targeted for degradation by 20S proteasomes, independently of ubiquitylation (Ben-Nissan and Sharon, 2014; Jariel-Encontre et al., 2008). An unfolded or intrinsically unstructured region appears to be a primary determinant of 20S targets, and hydrophobic stretches may enhance recognition and promote opening of the ring channel formed by the α-subunits of the proteasome core. Indeed, the N-terminal region of Msh4 is predicted to be largely unfolded, with patches of relatively high hydrophobicity (https://fold.weizmann.ac.il/fldbin/findex; https://iupred2a.elte.hu/; https://web.expasv.org/protscale/). Phosphorylation could act to locally disrupt hydrophobicity and/or induce folding, suggesting a simple biophysical impediment to degradation by 20S proteasomes. The mechanism described here for Msh4, i.e. phosphorylation-mediated inactivation of an intrinsically unstructured degron, appears to be shared with other ubiquitin-independent proteasomal targets such as phosphatidate phosphatase (Hsieh et al., 2015) and the Fos-family transcription factors c-Fos and Fra-1 (Jariel-Encontre et al., 2008).

DDK Is A Key Effector of Meiotic Prophase

DDK is the primary effector kinase for the major events of meiosis. In addition to stabilizing Msh4 to activate MutSγ for crossing over, DDK facilitates meiotic S-phase (Valentin et al., 2006); triggers DSBs and couples their formation to the passage of replication forks (Lam and Keeney, 2014); promotes synapsis and crossing over via phosphorylation of Zip1 (Chen et al., 2015); enables progression beyond pachytene by removing the Sum1 repressive complex from the *NDT80* promoter (Lo et al., 2008); drives the destruction of SCs (Argunhan et al., 2017); helps recruit monopolin to kinetochores to enable mono-orientation of homologs on the meiosis-I spindle (Lo et al., 2008; Matos et al., 2008); and facilitates the cleavage of cohesin to allow homolog disjunction at meiosis-l (Katis et al., 2010).

Direct targeting of both Zip1 and Msh4 implies that DDK is a general activator of ZMM-mediated crossing over. However, the timing, requirements and modes of regulation are distinct. By contrast to Msh4, phosphorylation of Zip1 is an early event that depends on DSB formation but not later steps of recombination, and doesn't act by stabilizing Zip1 protein (Chen et al., 2015). Moreover, DDK-mediated phosphorylation of Zip1 is inferred to function upstream of the other ZMMs. Consistent with this inference, Msh4 phosphorylation requires Zip1 (Figure 7B). Importantly, the upstream but indirect requirement for the Mek1 kinase in DDK-mediated Zip1 phosphorylation (Chen et al., 2015) explains why Msh4 phosphorylation is also Mek1 dependent.

Contingent Kinase Cascades Order The Events of Meiotic Prophase

While DKK appears to be the ultimate effector kinase for many prophase events, other kinases dictate its activity in space and time. CDK primes DDK phosphorylation of Mer2 to trigger DSB formation (Henderson et al., 2006; Sasanuma et al., 2008; Wan et al., 2008). DSB-dependent activation of $Mec1^{ATR}$/$Tel1^{A\text{T}\text{M}}$ locally activates Mek1 (Carballo et al., 2008), which promotes inter-homolog recombination via its direct targets (Callender et al., 2016; Niu et al., 2009), and indirectly activates synapsis and the ZMM pathway by licensing DDK to phosphorylate Zip1 and subsequently Msh4 (Chen et al., 2015)(this study). CDK, DDK and the meiosis-specific kinase Ime2 collectively target the Sum1 transcriptional repressor to help activate expression of the transcription factor Ndt80, allowing cells to progress beyond pachytene (Winter, 2012). The polo-like kinase Cdc5, whose expression is Ndt80 dependent, then collaborates with CDK and DDK to disassemble SCs (Argunhan et al., 2017; Sourirajan and Lichten, 2008). Cdc5 also collaborates with DDK to localize the monopolin complex to MI kinetochores (Lo et al., 2008; Matos et al., 2008). Finally, casein kinase δ/ε works with DDK to activate the cleavage of cohesin by separase and trigger the meiosis-l division (Katis et al., 2010). Understanding the spatial-temporal regulation of DDK with respect to the activation of ZMM-dependent crossing over, and its relationship to crossover control are important goals for the future.

EXPERIMENTAL PROCEDURES

Extended methods are described in the STAR Methods.

STAR Methods

LEAD CONTACT AND MATERIALS AVAILABILITY

Further information and requests for resources and reagents should be directed to and will be fulfilled by the Lead Contact Neil Hunter, nhunter@ucdavis.edu

EXPERIMENTAL MODEL AND SUBJECT DETAILS

The genotype of the diploid *Saccharomyces cerevisiae* strains (SK1 background) used in this study are listed Table S6.

Synthetic dropout and YPD solid and liquid media were prepared according to standard protocols (Owens et al., 2018; Sherman, 2002) SPS and SPM media for meiotic time courses were prepared as described (Owens et al., 2018). All yeast cultures were incubated at 30°C.

METHOD DETAILS

Yeast Strains and Tetrad Analysis.—Full genotypes are shown in Table S6. The *HIS4::LEU2* locus has been described (Hunter and Kleckner, 2001). The strain carrying chromosome III with eight linked intervals strain was described previously (Lao et al., 2013b). The strain with nine intervals located in three different chromosomes has been described (Oh et al., 2007). Tetrad analysis was performed using standard techniques as described (Perkins, 1949). Map distances and NPD ratios were calculated using Stahl Lab Online Tools (http://elizabethhousworth.com/StahlLabOnlineTools/). *msh4* phosphorylation site alleles were created by using QuikChange II Site-Directed Mutagenesis Kit (Agilent Technologies Inc, 200524) and confirmed by DNA sequencing by Eurofins Genomics LLC. All alleles were sequenced in their entirety to ensure that no additional mutations were introduced. The P_{cup1}-*MSH4* and P_{cup1}-*MSH5* copper-inducible expression cassettes were created by replacing the native promoters of the *MSH4* and *MSH5* genes with the *CUP1* promoter. P_{cup1}-*GFP* was created by replacing the *MSH4* ORF in the P_{cup1}-*MSH4* cassette with the *GFP* gene from plasmid pF6A-GFP-KanMX4.

Meiotic Time Courses and DNA Physical Assays.—Detailed protocols for meiotic time courses and DNA physical assays have been described (Owens et al., 2018). Meiotic progression was analyzed by fixing the cells in 40% ethanol, 0.1 M sorbitol, staining with DAPI. 100 cells were counted for each time point. Error bars show averages (± SD) from three to six experiments.

Immunoprecipitation and LC–MS/MS Analysis—For immunoprecipitation of Msh4-HA, all steps were performed at 4°C unless stated otherwise. 20g of pelleted cells harvested 6 hrs into meiosis were lysed in denaturing lysis buffer (1.85M NaOH, 7.4% 2-Mercaptoethanol), proteins were precipitated with 50% TCA followed by centrifugation for 20 min at 20,000 rpm. Pelleted cells were washed with 10 volume of cold acetone and resuspended in resuspension buffer (130µl 0.5M Tris PH 7.5, 6.5% SDS, 12% Glycerol + 13 µl 1M DTT). After 20 minutes of heating and mixing at 65°C, the extract was clarified by centrifugation for 10 minutes at 20,000 rpm. The clarified supernatant was diluted 1:10 in RIPA buffer (50mM Tris PH 7.4, 5mM EDTA, 150mM NaCI, 1% Triton X-100 +

complete™ Protease Inhibitor Cocktail; Millipore Sigma 11697498001), and incubated with 1ml anti-HA affinity matrix beads (Millipore Sigma 11815016001) for 4 hours. The beads were then washed 5 times with 10ml RIPA buffer and boiled in 500ul p2X Laemmli buffer for 5 minutes. Proteins were separated by standard SDS-PAGE, stained with Coomassie brilliant blue staining solution (0.04% CBB G-250, 10% ethanol, 2% orthophosphoric acid), and pertinent gel slices were excised and processed for tandem mass spectrometry by University of California, Davis Proteomics Core (UCDPC; http://proteomics.ucdavis.edu). Protein samples were digested with trypsin and cleaned up using a MacroSpin column. The peptides were then separated using a Proxeon Easy-nLC II HPLC (Thermo Scientific) and loaded into a O Exactive Orbitrap mass spectrometer with a Proxeon nanospray source (Thermo). Detected spectra and fragmentation profiles were matched against a Uniport *Saccharomyces cerevisiae* proteome database. Peptide matches were analyzed using Scaffold4.

Western Blotting Analysis—Whole cell extracts were prepared using the TCA extraction method, essentially as described (Johnson and Blobel, 1999). Samples were then analyzed by standard SDS-PAGE and Western analysis. Anti-HA monoclonal antibody (12CA5) (Millipore Sigma; 11583816001) was diluted 1:2,000 to detect msh4-3HA and Msh5–3HA; anti-GFP monoclonal antibody (B34) (Abcam ab73933) was diluted 1: 5,000 to detect GFP; Arp7 polyclonal antibody (Santa Cruz, SC-8960) was used at a 1: 10,000 dilution as a loading control. The antibodies used in cell fractionation assay (Figure 6) were anti-tubulin monoclonal antibody (10D8) (Santa Cruz sc-53646) diluted at 1: 5,000, and anti-Histone H3 (tri methyl K4) polyclonal antibody (Abcam ab8580) diluted at 1: 10,000. The anti-hapten antibody (Aceam, ab92570) used for the semisynthetic epitope method was diluted at 1: 2,000. The secondary antibodies were IRDye® 800CW Donkey anti-Mouse IgG (LI-COR, 925–32212), IRDye® 680LT Donkey anti-Goat IgG (LI-COR, 925–68024), IRDye® 680LT Donkey anti-Rabbit IgG (LI-COR, 925–68023) and IRDye® 800CW Donkey anti-Rabbit IgG (LI-COR, 925–32213). Membranes were imaged with Odyssey Infrared Imager (LI-COR). Quantification of protein bands was performed using Image Studio Lite Ver 4.0 software.

Yeast Cytology and Chromosome Spreading.—Meiotic cells were collected at indicated time points and then fixed and spread as described (Grubb et al., 2015; Loidl and Lorenz, 2009). Immunostaining was performed as described (Grubb et al., 2015). Chromosome spreads were incubated overnight at room temperature with anti-HA antibody (Millipore Sigma; 11583816001, 1:200) and anti-Zip1 antibody (gift from Dr. Akira Shinohara, 1:200) in 100ul TBS/BSA buffer (10mM Tris PH7.5, 150mM NaCI, 1% BSA), followed by incubation with goat fluorochrome-conjugated secondary antibodies for 1 hr at 37°C (anti-rabbit 568, A11036 Molecular Probes, 1:1000; and anti-mouse 488, A11029 Molecular Probes, 1:1000). Coverslips were mounted with Proong Gold antifade reagent (Invitrogen P36930). Digital images were captured using a Zeiss AxioPlan II microscope, Hamamatsu ORCA-ER CCD camera and analyzed using Volocity software. Scatterplots were generated using the Graphpad program in Prism.

Chromatin Fractionation Assay—The chromatin fractionation assay was performed as described (Kunoh and Habu, 2014).

Msh4-Msh5 expression constructs—For wild type Msh4-Msh5, the *MSH4* gene was amplified from genomic DNA of the S. *cerevisiae* SK1 strain using forward primer 258 (5′GGCTAGCTGCTAGCGGATCCATGAGTGAATCTAATCTATCTAG-3′) and reverse primer 259b (5′CGCAAATCAAGCTTTATTTTTCGAACTGCGGGTGGCTCCACTCGAGTTCTTCAAAATTTTCGATGAAG-3′). For mutant variants of the Msh4-Msh5 complex, the *msh4-3A* and *msh4-6A* genes were amplified from the corresponding mutant strains. The reverse primer includes a sequence coding for the Strep-Tactin II affinity tag to create a C-terminal fusion with Msh4. *MSH4* genes were cloned into pFB-GST-MLH1(Ranjha et al., 2014) using *Bam* HI and *Hind* III to create pFB-MSH4-strep. The *MSH5* gene was amplified from genomic DNA of the S. *cerevisiae* W303 strain using forward primer 265 (5′GGCTAGCTGCTAGCGGATCCATGTCCCATGAATGGCTCATAAG-3′) and reverse primer 266 (5′-CGCAAATCCTCGAGCCCGGGGCGAAGGAAATTTTTCAATTTAAGC-3′). *MSH5* was cloned into pFB-MBP-MLH3-his (Ranjha et al., 2014) using *BamYW* and *Xho*I restriction sites to create pFB-MSH5-his. Baculoviruses were prepared using Bac-to-Bac system (Invitrogen) according to manufacturer's instructions and Sf9 cells were co-infected with optimized ratios of both viruses to express Msh4 and Msh5 together as a heterodimer. The cells were harvested 52 hrs post-infection, pellets were washed with phosphate buffered saline, frozen in liquid nitrogen and stored at −80°C until use.

Protein Purification—To purify Msh4-Strep–Msh5-His complex, 3.2L (for wild-type Msh4) or 1L (for Msh4 mutants) Sf9 cells were harvested 52 hr after infection with 15 ml of high titer virus for each expression construct. Cell pellets were incubated with mixing for 30 mins with lysis buffer (50mM Tris, pH7.5, 2mM β-ME, 1mM EDTA, 1 mM PMSF, 1:400 (v/v) Sigma protease inhibitory mixture (P8340), 30 ug/ml Leupeptin, 20mM imidazole, 16% glycerol, 325 mM NaCI). The suspension was then centrifuged at 18 000 rpm for 3 0 min. Cleared extract was incubated with 5 ml recycled Ni-NTA resin on a roller for 1 hr, the resin was washed with NTA wash buffer (50mM Tris pH7.5, 2mM β-ME, 300mM NaCI, 10% glycerol, 1 mM PMSF, 10 ug/ml Leupeptine, 40mM imidazole), and eluted with NTA elution buffer (50mM Tris pH7.5, 2mM β-ME, 300mM NaCI, 10% glycerol, 1 mM PMSF, 250mM imidazole). The NiNTA eluates were then incubated with 1ml Strep-tactin resin for 1 hr, washed with Strep wash buffer (50 mM Tris pH 7.5, 2 mM β-mercaptoethanol, 10% glycerol, 1mM phenylmethylsulfonyl fluoride and 300mM NaCI), then with wash buffer II (50 mM Tris pH 7.5, 2 mM β-mercaptoethanol, 10% glycerol, 1mM phenylmethylsulfonyl fluoride and 150 mM NaCI) before eluting with Strep elution buffer (2.5mM desthiobiotin, 50mM Tris pH 7.5, 2mM β-mercaptoethanol, 10% glycerol, 1mM phenylmethylsulfonyl fluoride and 150mM NaCI). The sample was aliquoted, frozen in liquid nitrogen and stored at −80 °C. Cdc7-as3-FLAG was partially purified from meiotic cultures of *ndt80A* cells (strain NHY9625), as described (Chen et al., 2015). GST-Mek1-as was partially purified from strain NH520/pLW3 as described (Chen et al., 2015).

Inhibition of analogue-sensitive kinases—Meiotic cultures were split at 5hr, one half was treated with as-kinase inhibitor, and an equivalent volume of DMSO was added to the half. To inhibit Cdc7-as3, PP1 (Tocris, 1397) was added to a final concentration of 30μM. To inhibit Cdc28-as, 1-NM-PP1 (Santa Cruz, sc-203214) was added to a final concentration of 5μM. To inhibit Mek1-as, 1-NA-PP1 (Cayman Chemicals, 10954) was added to a final concentration of 10μM. To inhibit Hrr25-as, 1-NM-PP1 (Santa Cruz, sc-203214) was added to a final concentration of 5μM. Samples were then collected at indicated timepoints. TCA cell extracts prepared and Western blotting were performed and as described above.

In Vitro Kinase Assays—GST-Mek1-as kinase assays using the semisynthetic epitope system were performed as described (Chen et al., 2015), with 280 ng of the Msh4-strep–Msh5-his complex was added as substrate with or without 1uM 1-NA-PP1 to inhibit Mek1-as. For the Cdc7-as3FLAG kinase assays, 280 ng Msh4-strep–Msh5-his, msh4-3A-Strep–Msh5-his, or msh4-6A-Strep–Msh5-his were added as substrate. 20 uM PP1 (Tocris, 1397) was used as inhibitor of Cdc7-as-3FLAG. To purify Msh4 from kinase reactions, 100 μl kinase reactions were dialyzed using an Amicon Ultra-0.5 Centrifugal Filter Unit with Ultracel-30 membrane (Millipore Sigma, UFC503024), diluted with 500 ul of Strep wash buffer (50 mM Tris pH 7.5, 10 % glycerol, 1 mM PMSF and 300 mM NaCI), incubated with 20 μl resin of Strep-Tactin® Sepharose (IBA, 2-1201-002) for 1 hr at 4°C. The resin was washed 5 times with 1ml high salt wash buffer (50 mM NaH_2PO_4 pH 8, 10 % glycerol, 1 mM PMSF, 750mM NaCI) and 5 times with 1ml Strep wash buffer. An equal volume of 2x Laemmli sample buffer was added to the resin and incubated for 5 mins at 95°C. Samples were then analyzed by Western blotting. 10% of the kinase reactions were analyzed as loading controls using anti-Msh4 primary antibodes (a kind gift from Dr. Akira Shinohara).

In vitro Phosphatase Treatment—15ml of meiotic cells (strain NYH779) were harvested at 6hr, cell extracts were prepared as described in section “Immunoprecipitation and LC–MS/MS Analysis”, and Msh4-HA was immunoprecipitated with 30μl of anti-HA affinity matrix (Millipore Sigma 11815016001) as described above. The beads were divided into three aliquots: mock, phosphatase treatment and phosphatase + inhibitor. Dephosphorylation was carried out by mixing 10μl beads, 5μl 10X PMP buffer, 5μl 10mM $MnCl_2$, 2μl λ-phosphatase (400U/ul; New England Biolabs, P0753S), 28μl of H2O and incubating at 37 °C for 2hr. In the phosphatase inhibitor reaction, 10μl 1M NaF, 2μl 1M NaVCU and 5 μl 10X PhosStop (Millipore Sigma, 4906845001) were added. Phosphatase reactions were stopped by mixing with an equal volume of 2x Laemmli sample buffer and immediately heating at 95°C for 5 min. Western analysis was then performed as described above.

Cycloheximide Chase Assay—100 mg/ml Cycloheximide solution (Millipore Sigma, C7698) was added at 1: 1,000 dilution to vegetative cell cultures in log phase (OD ~0.3-0.5) for a final concentration of 100 μg/ml. 1ml of culture was harvested at indicated time points and processed for protein extraction and Western analysis as descried above.

MG132 treatment for proteasome inhibition in vivo—Meiotic cell cultures of *MSH4/MSH4 pdr5Δ/pdr5Δ* (NHY 7643) and *msh4-6A/msh4-6A pdr5Δ/pdr5Δ* (NHY 7812

cells were treated with 25 μM MG 132 (and equivalent volume of DMSO was added to control cultures) at 2 hrs. The *pdr5Δ* mutation sensitizes strains to inhibition by MG132. Samples were collected at indicated time points and processed for Western analysis, as described above. For vegetative cultures, *pdr5Δ/pdr5Δ* derivatives were treated with 25 μM MG132 at log phase (OD ~0.3-0.5) and samples collected after 1 hr.

Purification of proteasomes—20S proteasomes were purified from yeast expressing TAP-tagged Pre1 using IgG-Sepharose affinity chromatography (MP Biomedical, SKU 0855961) as described (Leggett et al., 2005). The protein A tag was cleaved using 6His-TEV protease (New England Biolabs, P8112S), which was then removed via Ni-NTA agarose chromatography (QIAGEN, 30210). Protein content was estimated by the Bradford method.

Proteasomal degradation *in vitro*—Msh4/5 (20 nM) was incubated with purified 20S proteasomes (50 nM) at 30°C in a reaction mixture containing 50 mM Tris-HCI (pH 7.5), 150mM NaCI, 0.02% SDS, 1mM $MgCl_2$. Where indicated, MG132 (dissolved in 2% dimethyl sulfoxide) was added at a final concentration of 100 μM to inhibit proteasome activity. Reactions were sampled at indicated time points, terminated by boiling in an equal volume of 4X SDS Laemmli buffer, and analyzed by SDS-PAGE and Western blotting.

Co-immunoprecipitation of Msh4-Msh5 complexes from meiotic yeast samples—Indicated strains carrying C-terminally tagged msh4-3HA and Msh5–3FLAG were induced to undergo meiosis. Cells from 50 mL samples were harvested after 6 hrs, washed with dH_2O and snap-frozen in liquid nitrogen. Frozen cells were ground in a FreezerMill Cryogenic Grinder (SPEX SamplePrep, 6970EFM) and the cell powder was incubated with a equal volume of lysis buffer (50 mM HEPES-KOH (pH 7.8, 150 mM KCI.1 mM EDTA, 10% glycerol, 0.005% NP-40, 0.05% Tween-20, complete™ Protease Inhibitor Cocktail) for 2 hrs at 4°C. The cell extract was clarified by centrifugation for 1 hr at 40,000g and the supernatant incubated with 30 μl of anti-FLAG M2 Magnetic Beads (Sigma Aldrich, M8823) for 4 hrs at 4°C. Beads were then washed five time with lysis buffer. Immuno-precipitated proteins were then eluted by boiling in 20 μl of 2X Laemmli buffer for 5 min and analyzed by western blotting.

Analysis of MutSγ-DDK interaction in solution—7 μM purified Msh4-Strep–Msh5-His (above) was added to 500 μl binding buffer (50 mM Tris-HCI pH 7.5, 100 mM NaCI, 10% (v/v) glycerol, 0.1 % Triton X-100, 10 mM $MgCl_2$, 1 mM PMSF and protease inhibitors) and filtered through an Amicon Ultra-0.5 Centrifugal Filter Unit with Ultracel-30 membrane (Millipore Sigma, UFC503024) to remove excess desthiobiotin. 20 μM partially purified Cdc7–3FLAG and 20 μl Strep-Tactin® Sepharose resin (IBA, 2-1201-002) were added and the mixture was incubated with end-to-end shaking for 3 hrs at 4°C. The Strep-Tactin resin was washed five times with 500 μl binding buffer and bound proteins eluted by boiling in 20 μl 2X Laemmli buffer. Proteins were analyzed by SDS-PAGE and Western blotting with anti-Msh4 and anti-FLAG M2 (Sigma Aldrich, F1804) antibodies.

EMSA—DNA substrates were prepared as described (Ranjha et al., 2014) except that the oligonucleotides were biotinylated at 3’ end and blocked by addition of streptavidin immediately before binding reactions were performed. DNA binding reactions (15 μl)

comprised 25 mM Hepes pH7.8, 5 mM magnesium chloride, 5% glycerol, 1 mM DTT, 50 μg/ml BSA, 15 nM Streptavidin, 0.5 nM of P32-labeled DNA substrate and 30 nM Msh4-Msh5 protein or its phosphomimetic variants. The reactions were assembled and incubated on ice for 15 mins followed by the addition of EMSA loading dye (5 μl) containing 50% glycerol, and 0.25% bromophenol blue. The products were separated on 4% native PAGE at 4°C. The gels were then dried, exposed to storage phosphor screens (GE Healthcare Life Sciences) and scanned using a Phosphorimager (Typhoon FLA 9500, GE Healthcare Life Sciences). DNA-binding efficiency was quantitated using Imagequant (GE Healthcare Life Sciences).

QUANTIFICATION AND STATISTICAL ANALYSIS

Most data are presented as means ± SEM or SD and represent at least three independent experiments. Statistical tests, *P* and *n* values are described in the figures and figure legends

DATA AND CODE AVAILABILITY

This study did not generate or analyze any datasets or code.

Supplementary Material

Refer to Web version on PubMed Central for supplementary material.

ACKNOWLEDGEMENTS

We thank members of the Hunter Lab, David Morgan (UCSF) and Kevan Shokat (UCSF) for support and discussions. This work was supported by NIH NIGMS grant GM074223 to N.H. and GM050717 to N.M.H. S.T. was supported by an NIH NIEHS-funded training program in Environmental Health Sciences (T32 ES007058). N.H. is an Investigator of the Howard Hughes Medical Institute.

REFERENCES

Agarwal S, and Roeder GS (2000). Zip3 provides a link between recombination enzymes and synaptonemal complex proteins. Cell 102, 245–255. [PubMed: 10943844]

Ahuja JS, Sandhu R, Mainpal R, Lawson C, Henley H, Hunt PA, Yanowitz JL, and Borner GV (2017). Control of meiotic pairing and recombination by chromosomally tethered 26S proteasome. Science 355, 408–411. [PubMed: 28059715]

Allers T, and Lichten M (2001). Differential timing and control of noncrossover and crossover recombination during meiosis. Cell 106, 47–57. [PubMed: 11461701]

Argunhan B, Leung WK, Afshar N, Terentyev Y, Subramanian VV, Murayama Y, Hochwagen A, Iwasaki H, Tsubouchi T, and Tsubouchi H (2017). Fundamental cell cycle kinases collaborate to ensure timely destruction of the synaptonemal complex during meiosis. The EMBO journal 36, 2488–2509. [PubMed: 28694245]

Ben-Nissan G, and Sharon M (2014). Regulating the 20S proteasome ubiquitin-independent degradation pathway. Biomolecules 4, 862–884. [PubMed: 25250704]

Borner GV, Kleckner N, and Hunter N (2004). Crossover/noncrossover differentiation, synaptonemal complex formation, and regulatory surveillance at the leptotene/zygotene transition of meiosis. Cell 117, 29–45. [PubMed: 15066280]

Brown MS, and Bishop DK (2015). DNA strand exchange and RecA homologs in meiosis. Cold Spring Harbor perspectives in biology 7, a016659.

Callender TL, Laureau R, Wan L, Chen X, Sandhu R, Laljee S, Zhou S, Suhandynata RT, Prugar E, Gaines WA, et al. (2016). Mek1 down regulates Rad51 activity during yeast meiosis by phosphorylation of Hed1. PLoS genetics 12, e1006226. [PubMed: 27483004]

Carballo JA, Johnson AL, Sedgwick SG, and Cha RS (2008). Phosphorylation of the axial element protein Hop1 by Mec1/Tel1 ensures meiotic interhomolog recombination. Cell 132, 758–770. [PubMed: 18329363]

Chen X, Suhandynata RT, Sandhu R, Rockmill B, Mohibullah N, Niu H, Liang J, Lo HC, Miller DE, Zhou H, et al. (2015). Phosphorylation of the synaptonemal complex protein Zip1 regulates the crossover/noncrossover decision during yeast meiosis. PLoS biology 13, e1002329. [PubMed: 26682552]

Cheng CH, Lo YH, Liang SS, Ti SC, Lin FM, Yeh CH, Huang HY, and Wang TF (2006). SUMO modifications control assembly of synaptonemal complex and polycomplex in meiosis of Saccharomyces cerevisiae. Genes & development 20, 2067–2081. [PubMed: 16847351]

De Muyt A, Jessop L, Kolar E, Sourirajan A, Chen J, Dayani Y, and Lichten M (2012). BLM helicase ortholog Sgs1 is a central regulator of meiotic recombination intermediate metabolism. Molecular cell 46, 43–53. [PubMed: 22500736]

De Muyt A, Pyatnitskaya A, Andreani J, Ranjha L, Ramus C, Laureau R, Fernandez-Vega A, Holoch D, Girard E, Govin J, et al. (2018). A meiotic XPF-ERCC1-like complex recognizes joint molecule recombination intermediates to promote crossover formation. Genes & development 32, 283–296. [PubMed: 29440262]

De Muyt A, Zhang L, Piolot T, Kleckner N, Espagne E, and Zickler D (2014). E3 ligase Hei10: a multifaceted structure-based signaling molecule with roles within and beyond meiosis. Genes & development 28, 1111–1123. [PubMed: 24831702]

Duroc Y, Kumar R, Ranjha L, Adam C, Guerois R, Md Muntaz K, Marsolier-Kergoat MC, Dingli F, Laureau R, Loew D, et al. (2017). Concerted action of the MutLbeta heterodimer and Mer3 helicase regulates the global extent of meiotic gene conversion. eLife 6.

Franklin FC, Higgins JD, Sanchez-Moran E, Armstrong SJ, Osman KE, Jackson N, and Jones GH (2006). Control of meiotic recombination in Arabidopsis: role of the MutL and MutS homologues. Biochem Soc Trans 34, 542–544. [PubMed: 16856855]

Guiraldelli MF, Felberg A, Almeida LP, Parikh A, de Castro RO, and Pezza RJ (2018). SHOC1 is a ERCC4-(HhH)2-like protein, integral to the formation of crossover recombination intermediates during mammalian meiosis. PLoS genetics 14, e1007381. [PubMed: 29742103]

Henderson KA, Kee K, Maleki S, Santini PA, and Keeney S (2006). Cyclin-dependent kinase directly regulates initiation of meiotic recombination. Cell 125, 1321–1332. [PubMed: 16814718]

Hollingsworth NM, Ponte L, and Halsey C (1995). MSH5, a novel MutS homolog, facilitates meiotic reciprocal recombination between homologs in Saccharomyces cerevisiae but not mismatch repair. Genes & development 9, 1728–1739. [PubMed: 7622037]

Hsieh LS, Su WM, Han GS, and Carman GM (2015). Phosphorylation regulates the ubiquitin-independent degradation of yeast Pah1 phosphatidate phosphatase by the 20S proteasome. The Journal of biological chemistry 290, 11467–11478. [PubMed: 25809482]

Humphryes N, Leung WK, Argunhan B, Terentyev Y, Dvorackova M, and Tsubouchi H (2013). The Ecm11-Gmc2 complex promotes synaptonemal complex formation through assembly of transverse filaments in budding yeast. PLoS genetics 9, e1003194. [PubMed: 23326245]

Hunter N (2015). Meiotic Recombination: The Essence of Heredity. Cold Spring Harbor perspectives in biology 7.

Hunter N, and Kleckner N (2001). The single-end invasion: an asymmetric intermediate at the double-strand break to double-holliday junction transition of meiotic recombination. Cell 106, 59–70. [PubMed: 11461702]

Jagut M, Hamminger P, Woglar A, Millonigg S, Paulin L, Mikl M, Dello Stritto MR, Tang L, Habacher C, Tam A, et al. (2016). Separable Roles for a *Caenorhabditis elegans* RMI1 Homolog in Promoting and Antagonizing Meiotic Crossovers Ensure Faithful Chromosome Inheritance. PLoS biology 14, e1002412. [PubMed: 27011106]

Jariel-Encontre I, Bossis G, and Piechaczyk M (2008). Ubiquitin-independent degradation of proteins by the proteasome. Biochimica et biophysica acta 1786, 153–177. [PubMed: 18558098]

Jessop L, Rockmill B, Roeder GS, and Lichten M (2006). Meiotic chromosome synapsis-promoting proteins antagonize the anti-crossover activity of Sgs1. PLoS genetics 2, e155. [PubMed: 17002499]

Jones GH (1984). The control of chiasma distribution. Symposia of the Society for Experimental Biology 38, 293–320. [PubMed: 6545727]

Katis VL, Lipp JJ, Imre R, Bogdanova A, Okaz E, Habermann B, Mechtler K, Nasmyth K, and Zachariae W (2010). Rec8 phosphorylation by casein kinase 1 and Cdc7-Dbf4 kinase regulates cohesin cleavage by separase during meiosis. Developmental cell 18, 397–409. [PubMed: 20230747]

Kaur H, De Muyt A, and Lichten M (2015). Top3-Rmi1 DNA single-strand decatenase is integral to the formation and resolution of meiotic recombination intermediates. Molecular cell 57, 583–594. [PubMed: 25699707]

Krishnaprasad GN, Anand MT, Lin G, Tekkedil MM, Steinmetz LM, and Nishant KT (2015). Variation in crossover frequencies perturb crossover assurance without affecting meiotic chromosome segregation in Saccharomyces cerevisiae. Genetics 199, 399–412. [PubMed: 25467183]

Lahiri S, Li Y, Hingorani MM, and Mukerji I (2018). MutSgamma-Induced DNA Conformational Changes Provide Insights into Its Role in Meiotic Recombination. Biophys J 115, 2087–2101. [PubMed: 30467025]

Lam I, and Keeney S (2014). Mechanism and regulation of meiotic recombination initiation. Cold Spring Harbor perspectives in biology 7, a016634. [PubMed: 25324213]

Lo HC, Wan L, Rosebrock A, Futcher B, and Hollingsworth NM (2008). Cdc7-Dbf4 regulates NDT80 transcription as well as reductional segregation during budding yeast meiosis. Molecular biology of the cell 19, 4956–4967. [PubMed: 18768747]

Macaisne N, Vignard J, and Mercier R (2011). SHOC1 and PTD form an XPF-ERCC1-like complex that is required for formation of class I crossovers. Journal of cell science 124, 2687–2691. [PubMed: 21771883]

Macqueen AJ, and Roeder GS (2009). Fpr3 and Zip3 ensure that initiation of meiotic recombination precedes chromosome synapsis in budding yeast. Current biology : CB 19, 1519–1526. [PubMed: 19765989]

Manhart CM, and Alani E (2016). Roles for mismatch repair family proteins in promoting meiotic crossing over. DNA repair 38, 84–93. [PubMed: 26686657]

Manhart CM, Ni X, White MA, Ortega J, Surtees JA, and Alani E (2017). The mismatch repair and meiotic recombination endonuclease Mlh1-Mlh3 is activated by polymer formation and can cleave DNA substrates in trans. PLoS biology 15, e2001164. [PubMed: 28453523]

Matos J, Lipp JJ, Bogdanova A, Guillot S, Okaz E, Junqueira M, Shevchenko A, and Zachariae W (2008). Dbf4-dependent CDC7 kinase links DNA replication to the segregation of homologous chromosomes in meiosis I. Cell 135, 662–678. [PubMed: 19013276]

Matsumoto S, and Masai H (2013). Regulation of chromosome dynamics by Hsk1/Cdc7 kinase. Biochem Soc Trans 41, 1712–1719. [PubMed: 24256280]

Mazina OM, Mazin AV, Nakagawa T, Kolodner RD, and Kowalczykowski SC (2004). Saccharomyces cerevisiae Mer3 helicase stimulates 3'-5' heteroduplex extension by Rad51; implications for crossover control in meiotic recombination. Cell 117, 47–56. [PubMed: 15066281]

Milano CR, Holloway JK, Zhang Y, Jin B, Smith C, Bergman A, Edelmann W, and Cohen PE (2019). Mutation of the ATPase Domain of MutS Homolog-5 (MSH5) Reveals a Requirement for a Functional MutSgamma Complex for All Crossovers in Mammalian Meiosis. G3 9, 1839–1850. [PubMed: 30944090]

Nakagawa T, and Kolodner RD (2002). Saccharomyces cerevisiae Mer3 is a DNA helicase involved in meiotic crossing over. Molecular and cellular biology 22, 3281–3291. [PubMed: 11971962]

Nguyen H, Labella S, Silva N, Jantsch V, and Zetka M (2018). C. elegans ZHP-4 is required at multiple distinct steps in the formation of crossovers and their transition to segregation competent chiasmata. PLoS genetics 14, e1007776. [PubMed: 30379819]

Nishant KT, Chen C, Shinohara M, Shinohara A, and Alani E (2010). Genetic analysis of baker's yeast Msh4-Msh5 reveals a threshold crossover level for meiotic viability. PLoS genetics 6.

Nishant KT, Plys AJ, and Alani E (2008). A mutation in the putative MLH3 endonuclease domain confers a defect in both mismatch repair and meiosis in *Saccharomyces cerevisiae*. Genetics 179, 747–755. [PubMed: 18505871]

Niu H, Wan L, Busygina V, Kwon Y, Allen JA, Li X, Kunz RC, Kubota K, Wang B, Sung P et al. (2009). Regulation of meiotic recombination via Mek1-mediated Rad54 phosphorylation. Molecular cell 36, 393–404. [PubMed: 19917248]

Novak JE, Ross-Macdonald PB, and Roeder GS (2001). The budding yeast Msh4 protein functions in chromosome synapsis and the regulation of crossover distribution. Genetics 158, 1013–1025. [PubMed: 11454751]

Oh SD, Lao JP, Hwang PY, Taylor AF, Smith GR, and Hunter N (2007). BLM ortholog, Sgs1, prevents aberrant crossing-over by suppressing formation of multichromatid joint molecules. Cell 130, 259–272. [PubMed: 17662941]

Pochart P, Woltering D, and Hollingsworth NM (1997). Conserved properties between functionally distinct MutS homologs in yeast. The Journal of biological chemistry 272, 30345–30349. [PubMed: 9374523]

Qiao H, Prasada Rao HB, Yang Y, Fong JH, Cloutier JM, Deacon DC, Nagel KE, Swartz RK, Strong E, Holloway JK, et al. (2014). Antagonistic roles of ubiquitin ligase HEI10 and SUMO ligase RNF212 regulate meiotic recombination. Nature genetics 46, 194–199. [PubMed: 24390283]

Rakshambikai R, Srinivasan N, and Nishant KT (2013). Structural insights into *Saccharomyces cerevisiae* Msh4-Msh5 complex function using homology modeling. PloS one 8, e78753. [PubMed: 24244354]

Ranjha L, Anand R, and Cejka P (2014). The Saccharomyces cerevisiae Mlh1-Mlh3 heterodimer is an endonuclease that preferentially binds to Holliday junctions. The Journal of biological chemistry 289, 5674–5686. [PubMed: 24443562]

Rao HB, Qiao H, Bhatt SK, Bailey LR, Tran HD, Bourne SL, Qiu W, Deshpande A, Sharma AN, Beebout CJ, et al. (2017). A SUMO-ubiquitin relay recruits proteasomes to chromosome axes to regulate meiotic recombination. Science 355, 403–407. [PubMed: 28059716]

Reynolds A, Qiao H, Yang Y, Chen JK, Jackson N, Biswas K, Holloway JK, Baudat F, de Massy B, Wang J, et al. (2013). RNF212 is a dosage-sensitive regulator of crossing-over during mammalian meiosis. Nature genetics 45, 269–278. [PubMed: 23396135]

Rockmill B, Fung JC, Branda SS, and Roeder GS (2003). The Sgs1 helicase regulates chromosome synapsis and meiotic crossing over. Current biology : CB 13, 1954–1962. [PubMed: 14614820]

Sasanuma H, Hirota K, Fukuda T, Kakusho N, Kugou K, Kawasaki Y, Shibata T, Masai H, and Ohta K (2008). Cdc7-dependent phosphorylation of Mer2 facilitates initiation of yeast meiotic recombination. Genes & development 22, 398–410. [PubMed: 18245451]

Shinohara M, Oh SD, Hunter N, and Shinohara A (2008). Crossover assurance and crossover interference are distinctly regulated by the ZMM proteins during yeast meiosis. Nature genetics 40, 299–309. [PubMed: 18297071]

Snowden T, Acharya S, Butz C, Berardini M, and Fishel R (2004). hMSH4-hMSH5 recognizes Holliday Junctions and forms a meiosis-specific sliding clamp that embraces homologous chromosomes. Molecular cell 15, 437–451. [PubMed: 15304223]

Sourirajan A, and Lichten M (2008). Polo-like kinase Cdc5 drives exit from pachytene during budding yeast meiosis. Genes & development 22, 2627–2632. [PubMed: 18832066]

Stahl FW, Foss HM, Young LS, Borts RH, Abdullah MF, and Copenhaver GP (2004). Does crossover interference count in Saccharomyces cerevisiae? Genetics 168, 35–48. [PubMed: 15454525]

Subramanian VV, and Hochwagen A (2014). The meiotic checkpoint network: step-by-step through meiotic prophase. Cold Spring Harbor perspectives in biology 6, a016675. [PubMed: 25274702]

Sym M, Engebrecht JA, and Roeder GS (1993). ZIP1 is a synaptonemal complex protein required for meiotic chromosome synapsis. Cell 72, 365–378. [PubMed: 7916652]

Sym M, and Roeder GS (1995). Zip1-induced changes in synaptonemal complex structure and polycomplex assembly. The Journal of cell biology 128, 455–466. [PubMed: 7860625]

Tang S, Wu MK, Zhang R, and Hunter N (2015). Pervasive and essential roles of the Top3-Rmi1 decatenase orchestrate recombination and facilitate chromosome segregation in meiosis. Molecular cell 57, 607–621. [PubMed: 25699709]

Thacker D, Mohibullah N, Zhu X, and Keeney S (2014). Homologue engagement controls meiotic DNA break number and distribution. Nature 510, 241–246. [PubMed: 24717437]

Valentin G, Schwob E, and Della Seta F (2006). Dual role of the Cdc7-regulatory protein Dbf4 during yeast meiosis. The Journal of biological chemistry 281, 2828–2834. [PubMed: 16319063]

Voelkel-Meiman K, Cheng SY, Morehouse SJ, and MacQueen AJ (2016). Synaptonemal Complex Proteins of Budding Yeast Define Reciprocal Roles in MutSgamma-Mediated Crossover Formation. Genetics 203, 1091–1103. [PubMed: 27184389]

Voelkel-Meiman K, Johnston C, Thappeta Y, Subramanian VV, Hochwagen A, and MacQueen AJ (2015). Separable Crossover-Promoting and Crossover-Constraining Aspects of Zip1 Activity during Budding Yeast Meiosis. PLoS genetics 11, e1005335. [PubMed: 26114667]

Voelkel-Meiman K, Taylor LF, Mukherjee P, Humphryes N, Tsubouchi H, and Macqueen AJ (2013). SUMO localizes to the central element of synaptonemal complex and is required for the full synapsis of meiotic chromosomes in budding yeast. PLoS genetics 9, e1003837. [PubMed: 24098146]

Wan L, Niu H, Futcher B, Zhang C, Shokat KM, Boulton SJ, and Hollingsworth NM (2008). Cdc28-Clb5 (CDK-S) and Cdc7-Dbf4 (DDK) collaborate to initiate meiotic recombination in yeast. Genes & development 22, 386–397. [PubMed: 18245450]

Winter E (2012). The Sum1/Ndt80 transcriptional switch and commitment to meiosis in Saccharomyces cerevisiae. Microbiology and molecular biology reviews : MMBR 76, 1–15. [PubMed: 22390969]

Woglar A, and Villeneuve AM (2018). Dynamic architecture of DNA repair complexes and the synaptonemal complex at sites of meiotic recombination. Cell 173, 1678–1691 e1616. [PubMed: 29754818]

Yang W, Junop MS, Ban C, Obmolova G, and Hsieh P (2000). DNA mismatch repair: from structure to mechanism. Cold Spring Harb Symp Quant Biol 65, 225–232. [PubMed: 12760036]

Yokoo R, Zawadzki KA, Nabeshima K, Drake M, Arur S, and Villeneuve AM (2012). COSA-1 reveals robust homeostasis and separable licensing and reinforcement steps governing meiotic crossovers. Cell 149, 75–87. [PubMed: 22464324]

Zakharyevich K, Ma Y, Tang S, Hwang PY, Boiteux S, and Hunter N (2010). Temporally and biochemically distinct activities of Exo1 during meiosis: double-strand break resection and resolution of double Holliday junctions. Molecular cell 40, 1001–1015. [PubMed: 21172664]

Zakharyevich K, Tang S, Ma Y, and Hunter N (2012). Delineation of joint molecule resolution pathways in meiosis identifies a crossover-specific resolvase. Cell 149, 334–347. [PubMed: 22500800]

Zhang L, Kohler S, Rillo-Bohn R, and Dernburg AF (2018). A compartmentalized signaling network mediates crossover control in meiosis. eLife 7, e30789 doi: 30710.37554/eLife.30789. [PubMed: 29521627]

Zhang L, Tang D, Luo Q, Chen X, Wang H, Li Y, and Cheng Z (2014). Crossover formation during rice meiosis relies on interaction of OsMSH4 and OsMSH5. Genetics 198, 1447–1456. [PubMed: 25278554]

Zickler D, and Kleckner N (2015). Recombination, pairing, and synapsis of homologs during meiosis. Cold Spring Harbor perspectives in biology 7, pii: a016626. doi:016610.011101/cshperspect.a016626.

Chan LY, and Amon A (2010). Spindle position is coordinated with cell-cycle progression through establishment of mitotic exit-activating and -inhibitory zones. Mol Cell 39, 444–454. [PubMed: 20705245]

Chen X, Suhandynata RT, Sandhu R, Rockmill B, Mohibullah N, Niu H, Liang J, Lo HC, Miller DE, Zhou H, et al. (2015). Phosphorylation of the synaptonemal complex protein Zip1 regulates the crossover/noncrossover decision during yeast meiosis. PLoS biology 13, e1002329. [PubMed: 26682552]

Grubb J, Brown MS, and Bishop DK (2015). Surface Spreading and Immunostaining of Yeast Chromosomes. J Vis Exp, e53081. [PubMed: 26325523]

Hunter N, and Kleckner N (2001). The single-end invasion: an asymmetric intermediate at the double-strand break to double-holliday junction transition of meiotic recombination. Cell 106, 59–70. [PubMed: 11461702]

Johnson ES, and Blobel G (1999). Cell cycle-regulated attachment of the ubiquitin-related protein SUMO to the yeast septins. The Journal of cell biology 147, 981–994. [PubMed: 10579719]

Kunoh T, and Habu T (2014). Chromatin Fractionation Assay in Fission Yeast bio-protocol 4, 5.

Lao JP, Cloud V, Huang CC, Grubb J, Thacker D, Lee CY, Dresser ME, Hunter N, and Bishop DK (2013a). Meiotic crossover control by concerted action of Rad51-Dmc1 in homolog template bias and robust homeostatic regulation. PLoS genetics 9, e1003978. [PubMed: 24367271]

Lao JP, Cloud V, Huang CC, Grubb J, Thacker D, Lee CY, Dresser ME, Hunter N, and Bishop DK (2013b). Meiotic Crossover Control by Concerted Action of Rad51-Dmc1 in Homolog Template Bias and Robust Homeostatic Regulation. PLoS Genetics 9.

Lee BH, and Amon A (2003). Role of Polo-like kinase CDC5 in programming meiosis I chromosome segregation. Science 300, 482–486. [PubMed: 12663816]

Leggett DS, Glickman MH, and Finley D (2005). Purification of proteasomes, proteasome subcomplexes, and proteasome-associated proteins from budding yeast. Methods in molecular biology 301, 57–70. [PubMed: 15917626]

Loidl J, and Lorenz A (2009). Analysis of Schizosaccharomyces pombe meiosis by nuclear spreading. Methods Mol Biol 558, 15–36. [PubMed: 19685316]

Ma Y, and Greider CW (2009). Kinase-independent functions of TEL1 in telomere maintenance. Molecular and cellular biology 29, 5193–5202. [PubMed: 19596790]

Malkova A, Swanson J, German M, McCusker JH, Housworth EA, Stahl FW, and Haber JE (2004). Gene conversion and crossing over along the 405-kb left arm of *Saccharomyces cerevisiae* chromosome VII. Genetics 168, 49–63. [PubMed: 15454526]

Oh SD, Lao JP, Hwang PYH, Taylor AF, Smith GR, and Hunter N (2007). BLM Ortholog, Sgs1, Prevents Aberrant Crossing-over by Suppressing Formation of Multichromatid Joint Molecules. Cell 130, 259–272. [PubMed: 17662941]

Owens S, Tang S, and Hunter N (2018). Monitoring Recombination During Meiosis in Budding Yeast. Methods Enzymol 601, 275–307. [PubMed: 29523236]

Perkins DD (1949). Biochemical Mutants in the Smut Fungus Ustilago Maydis. Genetics 34, 607–626. [PubMed: 17247336]

Ranjha L, Anand R, and Cejka P (2014). The Saccharomyces cerevisiae Mlh1-Mlh3 heterodimer is an endonuclease that preferentially binds to Holliday junctions. The Journal of biological chemistry 289, 5674–5686. [PubMed: 24443562]

Sherman F (2002). Getting started with yeast. Methods Enzymol 350, 3–41. [PubMed: 12073320]

Wach A, Brachat A, Pohlmann R, and Philippsen P (1994). New heterologous modules for classical or PCR-based gene disruptions in Saccharomyces cerevisiae. Yeast 10, 1793–1808. [PubMed: 7747518]

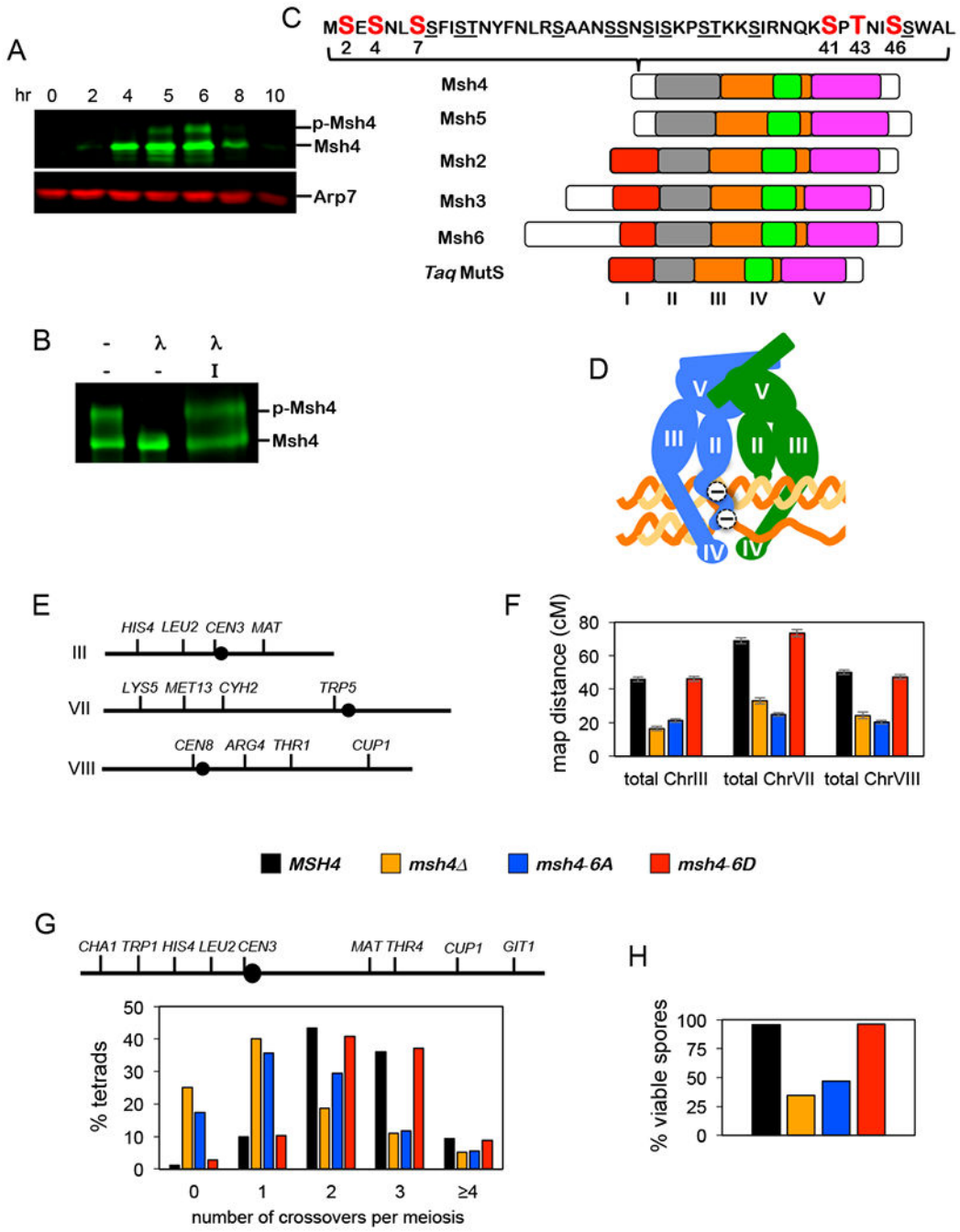

Figure 1. Phosphorylated of Msh4 is essential for its crossover function.

(A) Western analysis of Msh4 throughout meiosis. Arp7 is used throughout as a loading control (Sourirajan and Lichten, 2008). P-Msh4 indicates phosphorylated Msh4. (B) Lambda phosphatase treatment of immuno-precipitated Msh4. λ, phosphatase inhibitor; I, phosphatase inhibitor. (C) Positions of phosphorylation sites (red) mapped by LC-MS/MS. Underlined residues highlight the high S/T content of the Msh4 N-terminal region. Diagrams show protein domains of eukaryotic nuclear MutS homologs relative to *Thermus aquaticus* MutS (adapted from (Nishant et al., 2010). (D) Cartoon of rendering of predicted MutSγ

structure bound to a D-loop (Rakshambikai et al., 2013; Yang et al., 2000) highlighting the location of phosphorylation sites (represented as negative charges). Msh4 is colored blue, Msh5 is green. (E) Marker configurations in strains used to analyze recombination. *CEN3* is marked with the *ADE2* gene and *CEN8* is marked with *URA3* (Oh et al., 2007). (F) Cumulative frequencies of tetrads with gene conversions (non 2:2 segregations) for markers shown in (E). (G) Top: marker configuration in strains used to analyze crossover assurance for chromosome III. *CEN3* is heterozgously marked with the *LYS2 and URA3* (see Supplemental Information Table S6). Bottom: distributions of crossover classes (see Supplemental Information Table S5). (H) Spore viabilities of indicated strains (see Supplemental Information Table S1). Also see Supplemental Information Figures S1–S4.

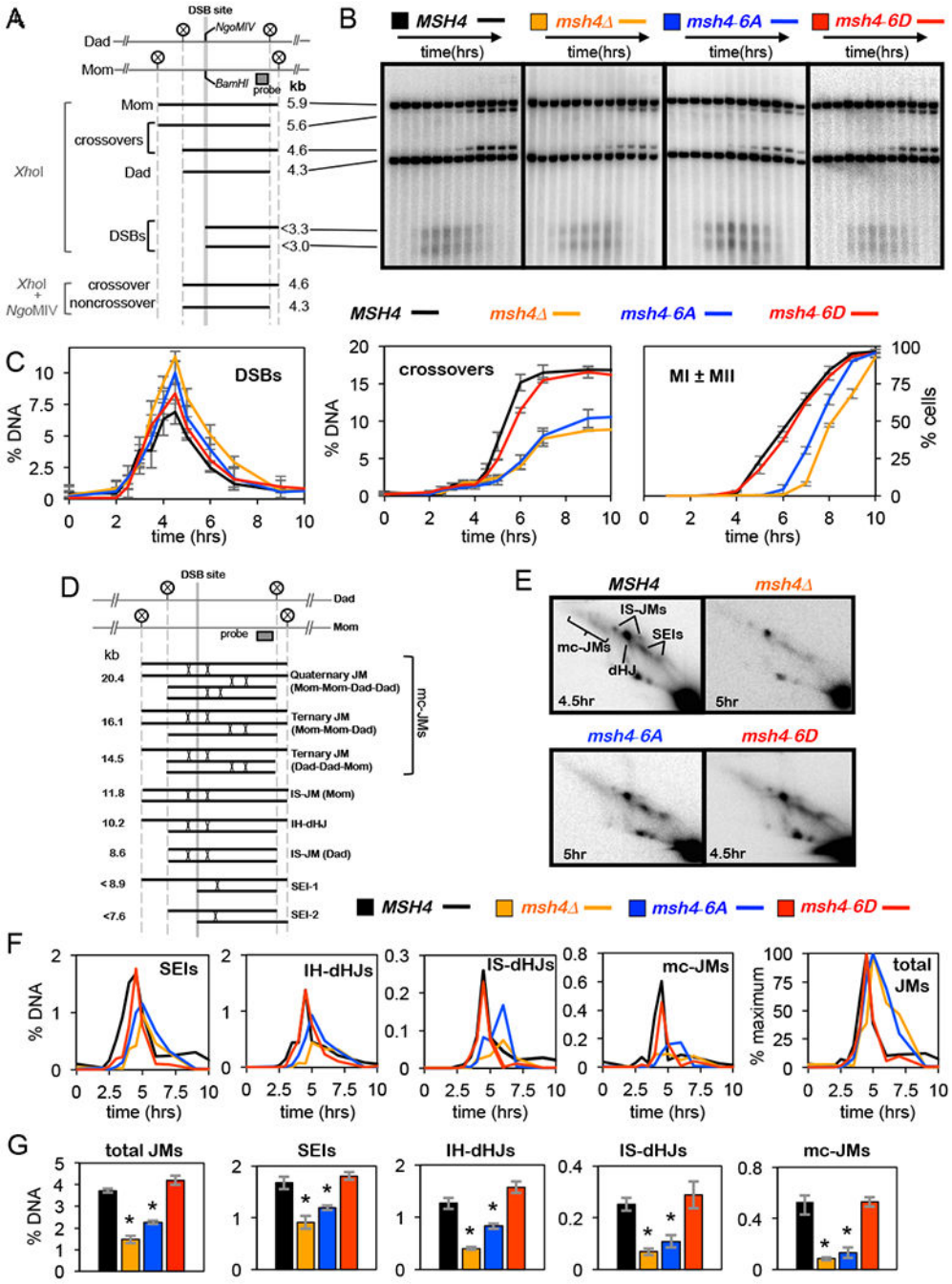

Figure 2. Physical analysis of the DNA events of meiotic recombination.

(A) Map of the *HIS4:LEU2* locus highlighting the DSB site, *Xho*I restriction sites (circled Xs) and the position of the probe used in Southern blotting. Sizes of diagnostic fragments are shown below. (B) Representative 1D gel Southern blot images for analysis of DSBs and crossovers. Time points are 0, 2, 2.5, 3, 3.5, 4, 4.5, 5, 6, 7, 9 and 11 hours. (C) Quantification of DSBs, crossovers and meiotic divisions. %DNA is percentage of total hybridizing DNA signal. MI ± MII is the percentage of cells that have completed one or both meiotic divisions. (D) Schematic of JM structures detected at the *HIS4:LEU2* locus. Positions of the

DSB site, diagnostic *Xho*I sites (circled Xs) and the Southern probe are shown. (E) Representative 2D gel Southern blot images for time points where JM levels peak. Positions of the various JM signals are indicated in the first panel. (F) Quantification of JM species over time. (G) Quantification of JM species at their peak levels from three independent time courses. IH-dHJs, inter-homolog dHJs; IS-JMs, intersister JMs; SEIs, single-end invasions; mcJMs, multi-chromatid JMs. Averages ± S.E. were calculated from three independent experiments. * $p<0.05$; Students t-test for comparisons to wild type.

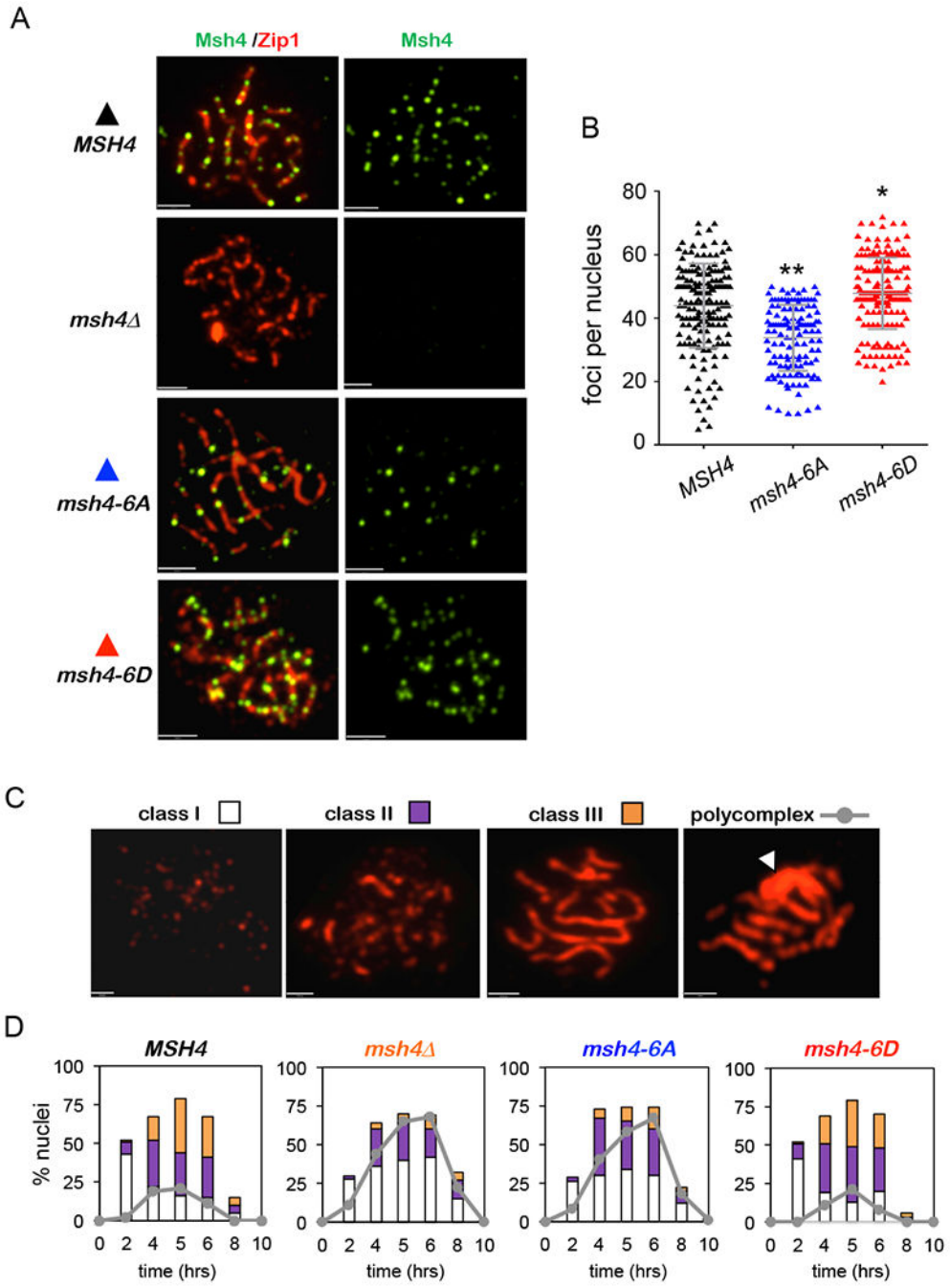

Figure 3. Chromosome synapsis and localization of MutSγ are facilitated by Msh4 phosphorylation.

(A) Representative images of spread meiotic nuclei immuno-stained for Msh4 (green) and Zip1 (red). (B) Quantification of Msh4 immuno-staining foci. Foci were counted in class II and class III nuclei (represented in panel C) such that equivalent stage nuclei were being compared, regardless of the altered synapsis seen in *msh4-6A* cells. ≥100 nuclei were scored for each strain. (C) Chromosome spreads showing representative examples of the three different Zip1 immuno-staining classes and a Zip1 polycomplex. (D) Quantification of Zip1 staining classes and polycomplexes. ≥100 nuclei were scored for each time point. *P<0.05;

** $P<0.01$ two tailed Mann Whitney test. Scale bars = 30 μm. Also see Supplemental Information Figure S5.

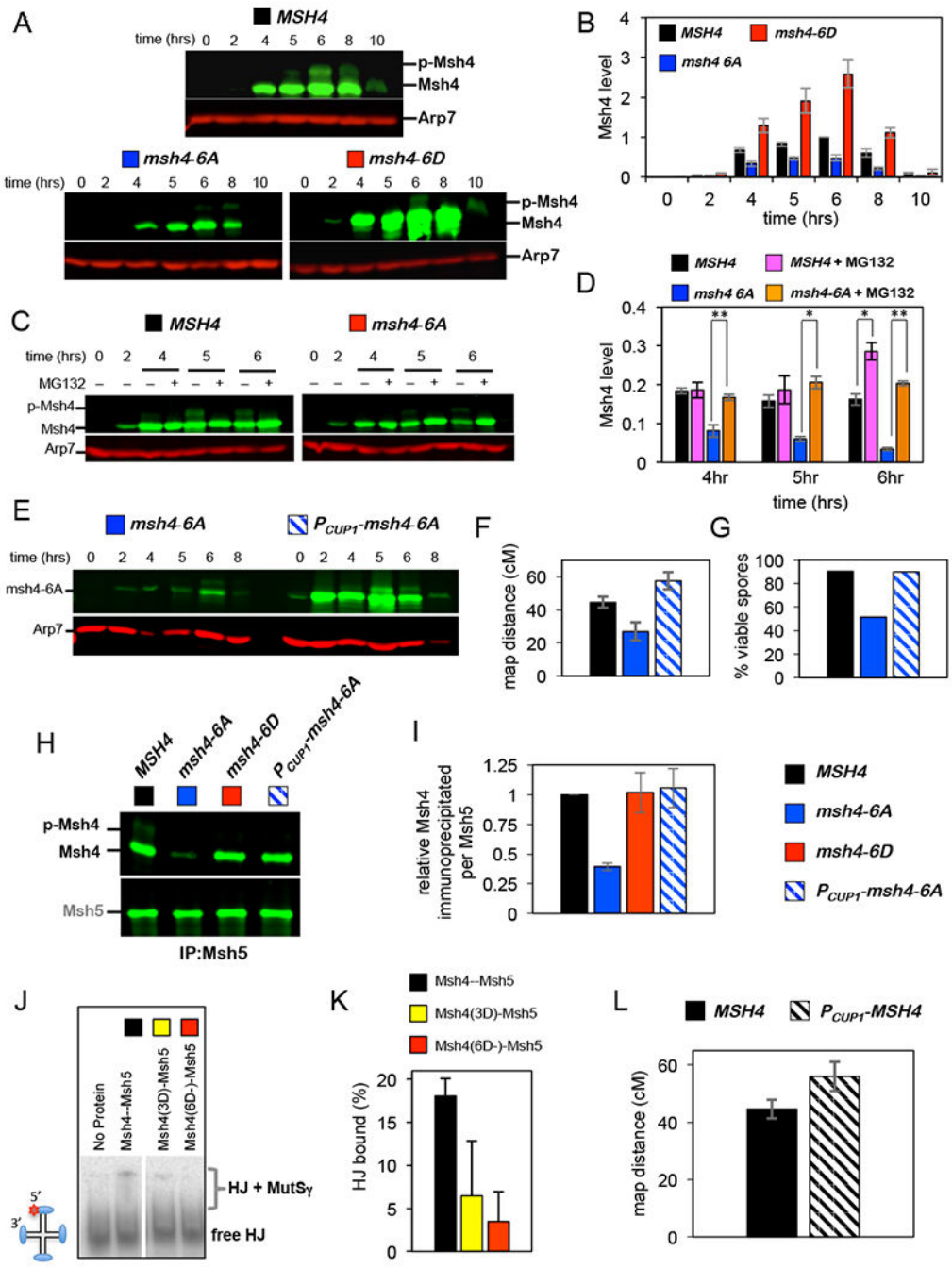

Figure 4. Phospho-regulated proteasomal proteolysis regulates the crossover function of Msh4

(A) Western analysis of Msh4 during meiosis in *MSH4, msh-6A* and *msh4-6D* strains. (B) Quantification of Msh4 protein relative to the Arp7 loading control. Averages ± S.E. were calculated from three independent experiments. (C) Western analysis of Msh4 with and without addition of the proteasome inhibitor, MG132, at 2 hrs. (D) Quantification of Msh4 protein with and without MG 132 treatment. (E) Western analysis of msh4-6A protein in the *msh4-6A* strain and following copper-induced overexpression in a P_{cup1}-*msh4-6A* strain. (F) Map distances (± S.E.) for intervals flanking the *HIS4::LEU2* recombination hotspot (see

Supplemental Information Figure S4B) in *MSH4, msh4-6A* and P_{cup1}-*msh4-6A* strains. (G) Spore viabilities of *MSH4, msh4-6A* and P_{cup1}-*msh4-6A* strains. (H) Western analysis of Msh4 and Msh5 protein levels in Msh5 immunoprecipitates. (I) Levels of Msh4 protein co-precipitated per Msh5 relative to wild type. (J) EMSA analysis of HJ binding by MutSγ complexes containing phosphomimetic Msh4 variants. (K) Quantification of HJ binding by MutSγ variants. (L) Map distances (± S.E.) for intervals flanking the *HIS4::LEU2* recombination hotspot in *MSH4* and P_{cup1}-*MSH4* strains. Averages ± S.E. were calculated from three independent experiments. * $p<0.05$, ** $p<0.01$; Students t-test. Also see Supplemental Information Figure S6.

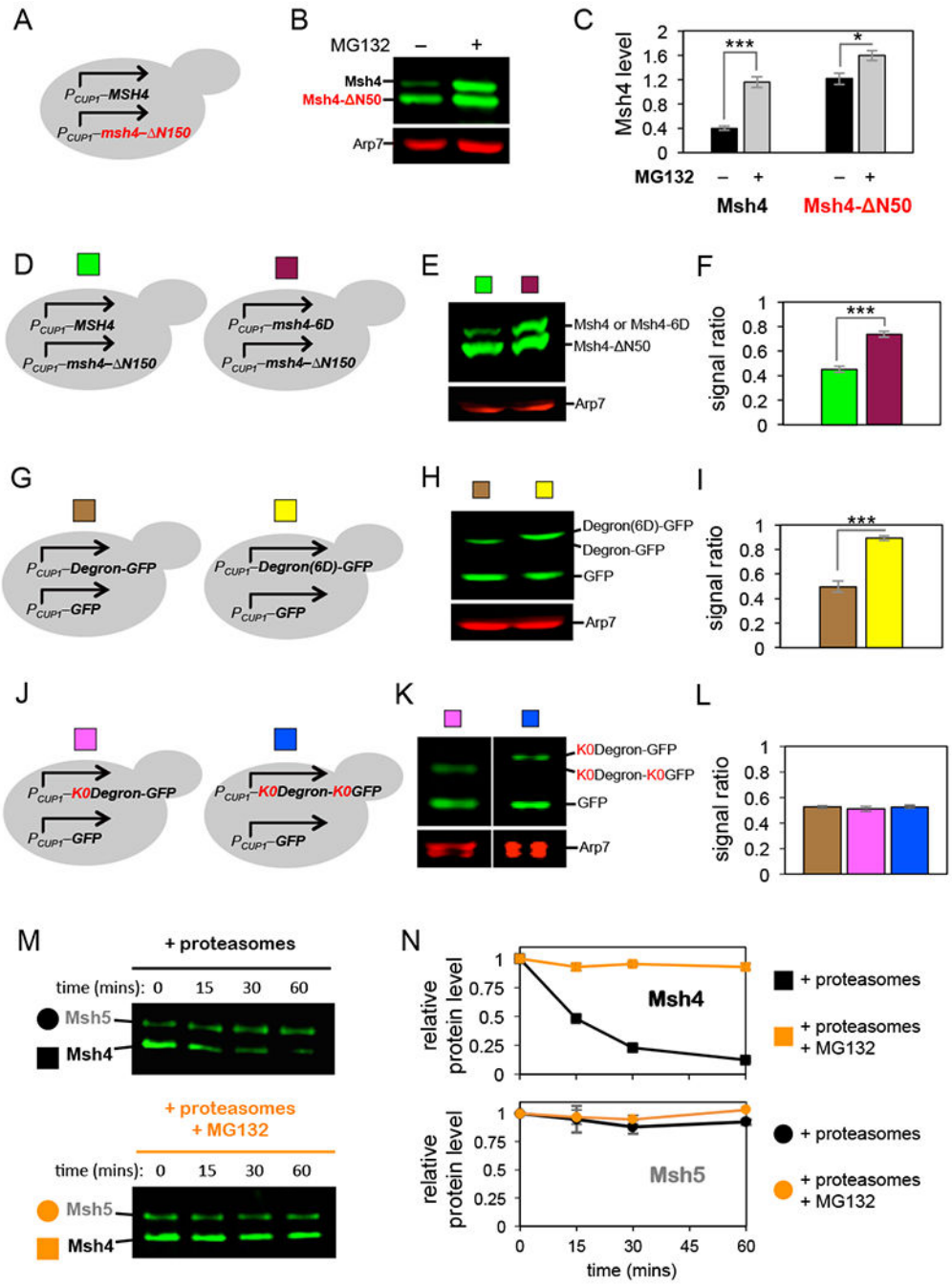

Figure 5. The Msh4 N-terminus encodes an autonomous degron that directly targets proteasomal degradation and is attenuated by phosphorylation.

(A) Experimental system for copper-inducible expression of Msh4 and Msh4-ΔN50 proteins in vegetative cells. (B) Western analysis of strains shown in (A) following copper induction, with and without MG132 treatment. (C) Quantification of the experiments represented in (A) and (B). Averages ± S.E. were calculated from four independent experiments. (D) Strains to compare co-expression of Msh4 and Msh4-ΔN50, with that of msh4-6D and Msh4-ΔN50 proteins. (E) Western analysis of stains shown in (D) following copper induction. (F) Quantification of experiments represented in (D) and (E). Average ratios ±

S.E. were calculated from four independent experiments. (G) Experimental systems for co-expression of GFP and the Msh4 N-terminal region ("degron") fused to GFP; or co-expresson of GFP and a phospho-mimetic derivative of the Msh4 N-terminal region ("degron 6D) fused to GFP. (H) Western analysis of the stains shown in (G) following copper induction. (I) Quantification of experiments represented in (G) and (H). Average ratios ± S.E. were calculated from four independent experiments. (J) Experimental strains co-expressing GFP and a mutant version of the Msh4 N-terminal region, with all lysines mutated to arginine, fused to GFP (K0Degron-GFP); or co-expressing GFP and a Msh4 degron-GFP fusion in which all lysines were mutated to arginines (K0Degron-K0GFP). (K) Western analysis of the strains shown in (J) following copper induction. (L) Quantification of experiments represented in (G) and (J). Average ratios ± S.E. were calculated from three independent Western blots. (M) Western analysis of *in vitro* proteolysis of MutSγ by 20S proteasomes ± MG132. (N) Quantification of the experiments represented in (M). Relative levels of Msh4 and Msh5 ± S.E. were calculated from triplicate experiments. Also see Supplemental Information Figures S7 and S8.

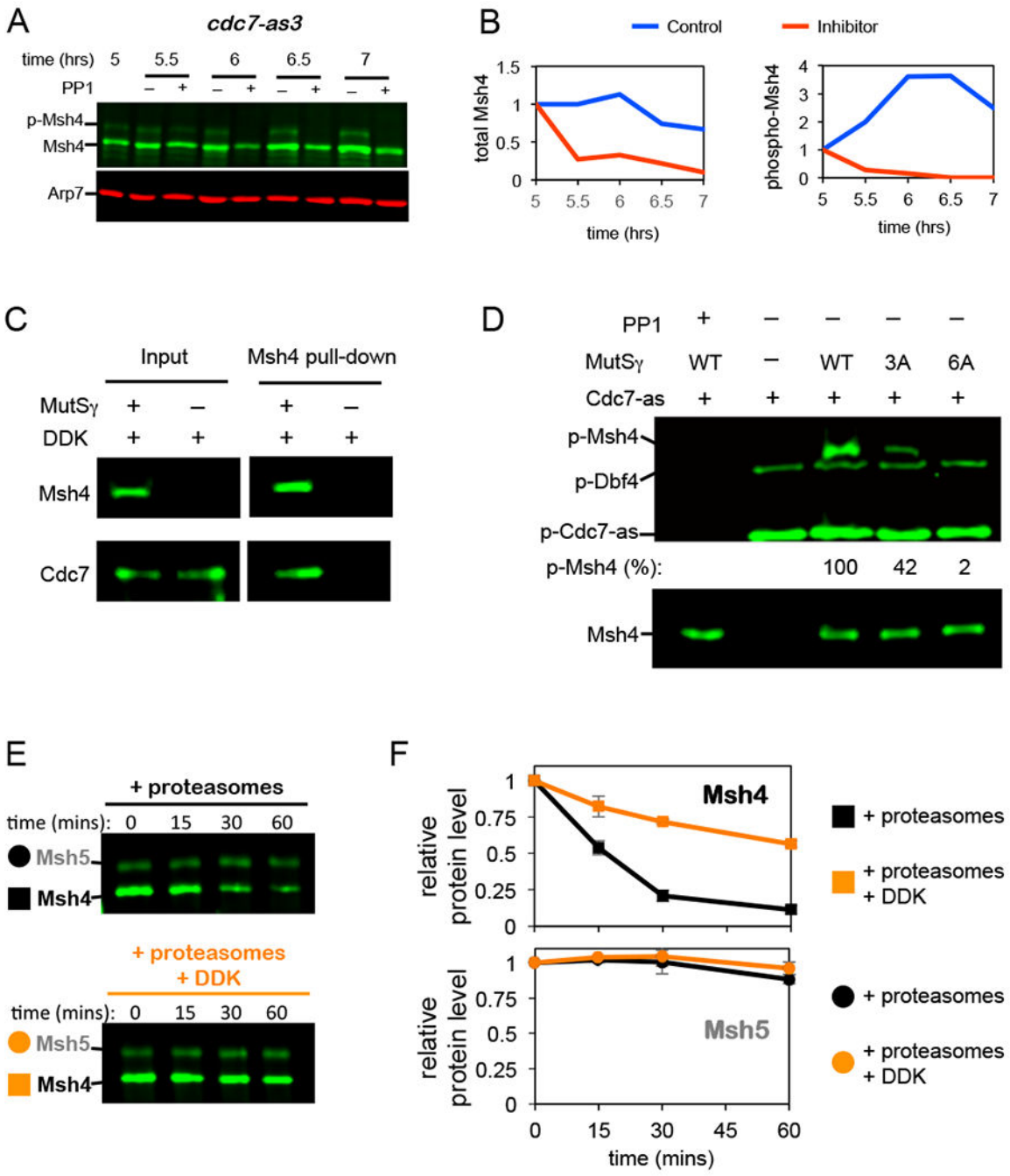

Figure 6. Msh4 is phosphorylated is catalyzed by DDK and antagonizes proteasomal degradation *in vitro*.

(A) Western analysis of Msh4 in strains containing the ATP-analog sensitive *cdc7-as* allele, with and without addition of the inhibitor PP1 at 5 hrs. (B) Relative levels of total and phosphorylated Msh4 quantified from the experiment shown in (A). Levels were normalized to the 5 hrs timepoint. (C) Western analysis demonstrating interaction between MutSγ and DDK (Cdc7-Dbf4) in solution. (D) Western analysis of Cdc7-as3-Dbf4 *in vitro* kinase assays with wild-type MutSγ or mutant derivatives containing S/T-A substitutions in the N-terminus of Msh4. The anti-thiophosphate ester (α-hapten) antibody recognizes

phosphorylation products of the semisynthetic epitope system. Phosphorylation efficiency was calculated relative to wild-type Msh4. In the lower panels, 10% of each reaction was probed for Msh4 as a loading control. (E) Western analysis of *in vitro* proteolysis of MutSγ by 20S proteasomes ± DDK (Cdc7-Dbf4). (F) Quantification of the experiments represented in (E). Relative levels of Msh4 and Msh5 ± S.E. were calculated from triplicate experiments. Also see Supplemental Information Figure S9 and S10.

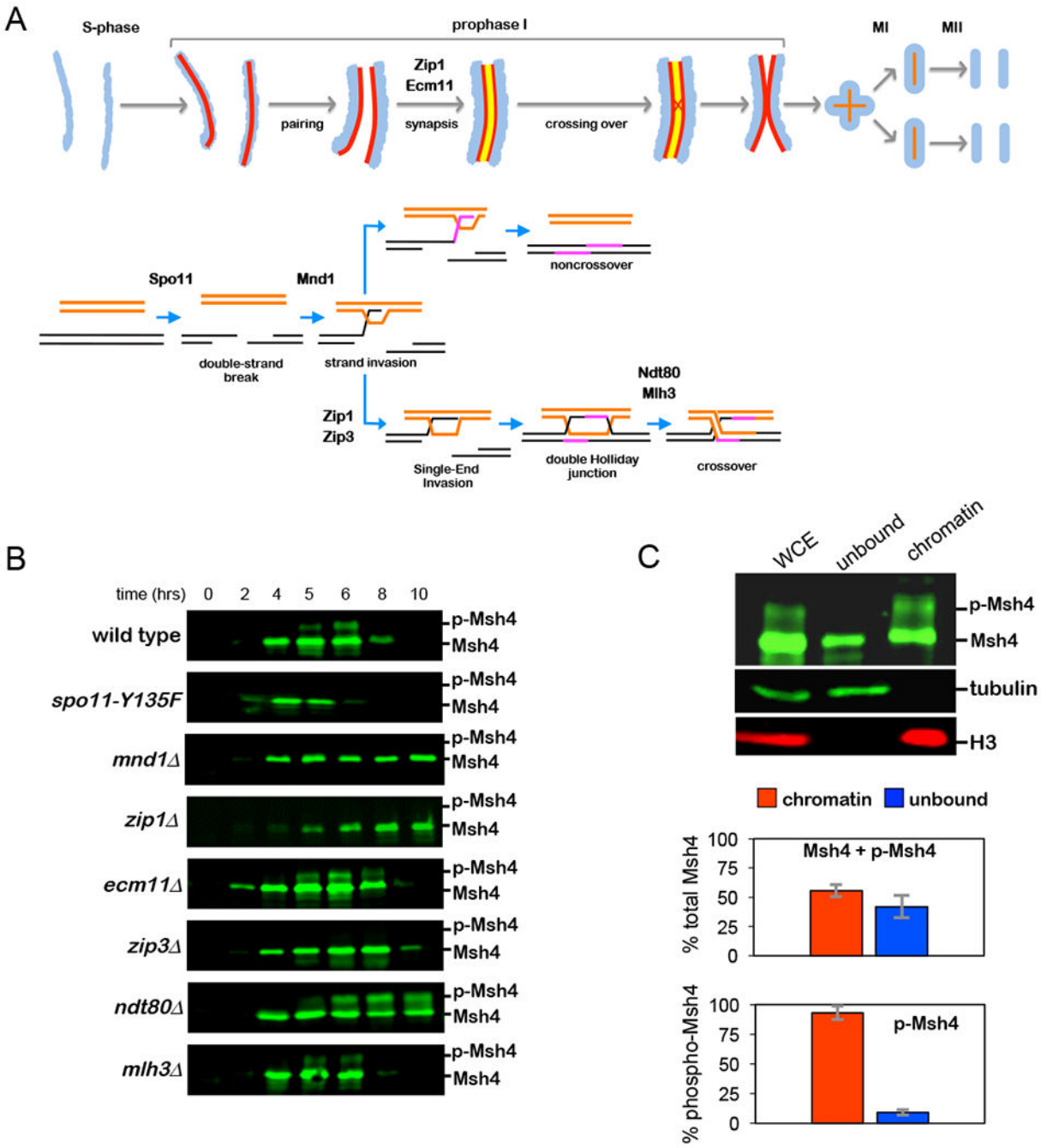

Figure 7. Genetic requirements of Msh4 phosphorylation.

(A) Chromosomal and recombination events of meiosis highlighting steps affected by the mutants analyzed in (B). Blue, chromatin; red lines, homolog axes; yellow line, synaptonemal complex central region. (B) Western analysis of Msh4 in the indicated mutant strains. (C) Top: Western analysis Msh4 in whole cell extracts ("WCE"), and extracts separated into soluble ("unbound") and chromatin fractions. Tubulin and histone H3 are markers for these two fractions. Bottom: Quantification of total Msh4 (top graph) and

phosphorylated Msh4 (bottom graph) in the two fractions. Means values ±S.E. were calculated from three independent experiments.

KEY RESOURCE TABLE

REAGENT or RESOURCE	SOURCE	IDENTIFIER
Antibodies		
Mouse Anti-HA Monoclonal Antibody,	Millipore Sigma	Cat#
Unconjugated, Clone 12CA5		11583816001, RRID:AB_514505
GFP antibody [B34]	Abcam	Cat# ab73933, RRID:AB_1268985
Monoclonal ANTI-FLAG® M2 antibody	Millipore Sigma	Cat# F3165, RRID: AB_259529
Arp7 (yN-20) antibody	Santa Cruz Biotechnology	Cat# sc-8960, RRID:AB_671731
αTubulin (10D8) antibody	Santa Cruz Biotechnology	Cat# sc-53646, RRID: AB_630403
Histone H3 (tri methyl K4) antibody	Abcam	Cat# ab8580, RRID: AB_306649
Thiophosphate ester antibody [51–8]	Abcam	Cat# ab92570, RRID:AB_10562142
IRDye® 800CW Donkey anti-Mouse IgG antibody	LI-COR Biosciences	Cat#:925-32212
IRDye® 680LT Donkey anti-Goat IgG antibody	LI-COR Biosciences	Cat#: 925-68024
IRDye® 680LT Donkey anti-Rabbit IgG antibody	LI-COR Biosciences	Cat#: 925-68023
IRDye® 800CW Donkey anti-Rabbit IgG antibody	LI-COR Biosciences	Cat#: 925-32213
Msh4 polyclonal antibody	Gift from Dr. A. Shinohara	N/A
Msh5 polyclonal antibody	Gift from Dr. A. Shinohara	N/A
Zip1 polyclonal antibody	Gift from Dr. A. Shinohara	N/A
Plasmids		
pFA6a-natMX4-pGAL1-3HA	Gift of Dr. A. Amon (Chan and Amon, 2010)	N/A
pFA6a-3HA-kanMX4		(Wach et al., 1994)
pFA6a-3HA-hphMX4		(Wach et al., 1994)
pFA6a-GFP-kanMX4		(Wach et al., 1994)
pU6H3FLAG	Gift from Dr. K. Ohta	N/A
Chemicals, Peptides, and Recombinant Proteins		
PP1	Tocris	Cat#: 1397
1-NM-PP1	Santa Cruz Biotechnology	Ca#: sc-203214
1-NA-PP1	Cayman Chemicals	Ca#: 10954
p-Nitrobenzyl mesylate	Abcam	Ca#: ab138910
PhosSTOP	Millipore Sigma	Ca#: 4906845001
Lambda Phosphatase	New England Biolabs,	Ca#: P0753S
Msh4-Strep-Msh5-His	This paper	N/A
Critical Commercial Assays		
QuikChange Lightning Site-Directed Mutagenesis Kit	Agilent Technologies	Ca#: 210518
Prime-It RmT Random Primer Labeling Kit	Stratagene	Ca#: 300392
Experimental Models: Organisms/Strains		
Saccharomyces cerevisiae; Individual genotypes see Table S6	N/A	N/A
Oligonucleootides		

REAGENT or RESOURCE	SOURCE	IDENTIFIER
See Table S7 for primers used in this paper		
Recombinant DNA		
pUC18-msh4-3HA-KanMX4 (pNH 599)	This paper	N/A
Software and Algorithms		
Volocity 6.3	Perkin Elmer	N/A
Image Studio Lite 4.0	LI-COR Biosciences	N/A
Scaffold 4.8.1	Proteome Software	N/A
Stahl Lab online tool	http://elizabethhousworth.com/StahlLabOnlineTools/	
Vassarstats online tool	http://vassarstats.net/newcs.html	